SOME CURRENT TOPICS IN CONDENSED MATTER PHYSICS 2016

M.E. MORA-RAMOS
R. PÉREZ-ÁLVAREZ
L. M. GAGGERO-SAGER
(editors)

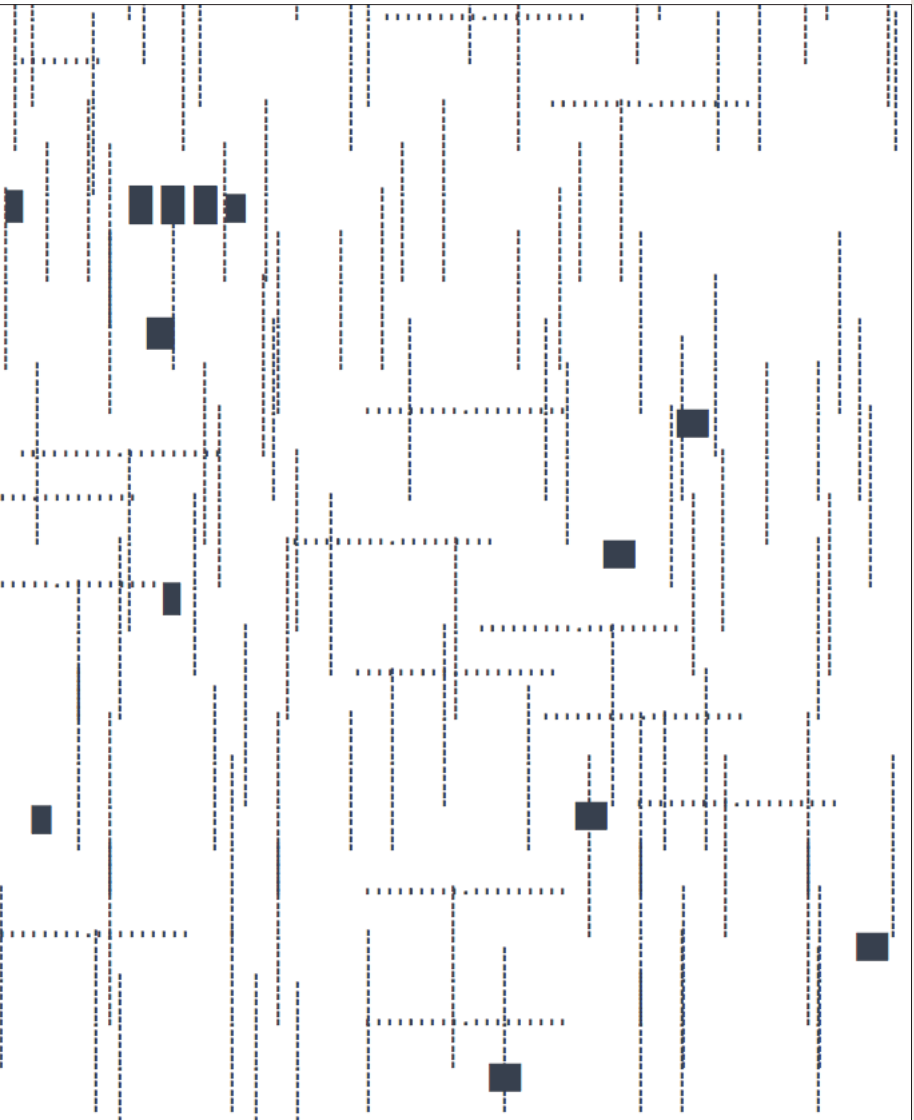

UNIVERSIDAD AUTÓNOMA DEL ESTADO DE MORELOS
Colección: *Contemporary Condensed Matter Physics: Selected Topics*

Some current topics in condensed matter physics

2016

M. E. Mora-Ramos, R. Pérez-Álvarez,
L. M. Gaggero-Sager
(Eds.)

Universidad Autónoma del Estado de Morelos
Cuernavaca. México
2018

Some current topics in condensed matter physics, 2016.
Colección: Contemporary Condensed Matter Physics: Selected Topics

D.R. 2018, Universidad Autónoma del Estado de Morelos
Av. Universidad 1001, Col. Chamilpa
62210, Cuernavaca, Morelos
publicaciones@uaem.mx
libros.uaem.mx

ISBN: 978-607-8519-73-6
ISBN (colección): 978-607-8434-78-7

Imagen de portada: Ernesto Ríos. De la serie Faebook dr@wings. Gráfica digital con teclado de celular, 2007

Cuerpo Académico de Física del Estado Sólido
Universidad Autónoma del Estado de Morelos

Foreword

For some years, professors belonging to the Group of Solid State Physics in the Morelos Autonomous State University (UAEM), have edited a series of compilations of selected talks at the Workshop of Molecular and Condensed Matter Physics, held at UAEM since 2008 (http://web.fc.uaem.mx/ tallerfmcm/temas.htm). The present is the fourth of this series of electronic books, which corresponds to the selection made in 2016. It contains some recent contributions in several areas of the research frontier in Condensed Matter Physics.

Since the first edition we have decided to keep the bilingual format (english-spanish) with the purpose of achieving a wider diffusion of the contents via electronic means.

Cuernavaca, Mexico. May 2017

M. E. Mora-Ramos
(memora@uaem.mx)
R. Pérez-Álvarez (rpa@uaem.mx)
L. M. Gaggero-Sager (lgaggero@uaem.mx)

Durante varios años, un grupo de profesores del Cuerpo Académico de Física del Estado Sólido de la Universidad Autónoma del Estado de Morelos, hemos compilado algunas de las conferencias impartidas en el Taller de Física de la Materia Condensada y Molecular, que se celebra desde 2008 en predios de la mencionada Instituci n. Luego de la publicación de los dos primeros volúmenes (http://web.fc.uaem.mx/ tallerfmcm/temas.htm) de esta serie de libros electrónicos, presentamos a la comunidad cuarto, correspondiente a la selección del año 2016. Esta vez, las contribuciones abarcan áreas de actividad de vanguardia de la Física de la Materia Condensada que no hab an sido abordadas en los libros anteriores.

Como comentamos en el prefacio del primer volumen de la serie, hemos mantenido con toda intención el formato bilingüe (español-inglés), en aras de que los materiales publicados puedan encontrar mayor difusión vía internet.

Cuernavaca, México. May 2017

M. E. Mora-Ramos (memora@uaem.mx)
R. Pérez-Álvarez (rpa@uaem.mx)
L. M. Gaggero-Sager (lgaggero@uaem.mx)

Contents

Anomalous diffusion in phase space: Relation to the entropy growth rate

Oscar Sotolongo-Costa, Oscar Sotolongo-Grau, L. M. Gaggero-Sager and I. Rodríguez-Vargas

Abstract

In this work it is shown that the time dependence of entropy can be intricate, more than the well-known linear dependence for chaotic systems. With the help of fractional calculus and considering a phase space with anomalous diffusion a close expression for the entropy was derived. This expression is quite general, since the equiprobability postulate is not longer assumed, the system dynamic in the phase space is not necessarily Markovian and the system is not in a steady state at all. Different possibilities for the time evolution of entropy by considering different features of the phase space and processes involved in the system dynamic are obtained.

En este trabajo se muestra que la dependencia temporal de la entropía puede ser compleja, mucho más incluso que la bien conocida dependencia lineal para sistemas caóticos. Con la ayuda del cálculo fraccionario y considerando un espacio de fase con difusión anómala se pudo derivar analíticamente una expresión para la entropía como función del tiempo. Esta expresión es general, ya que en ningún momento se asume el postulado de iguales probabilidades a priori, la dinámica del sistema en el espacio de fase no necesariamente es Markoviana e igualmente el sistema no está necesariamente en un estado estacionario. También se presentan

(OSC, IRV) Centro de Investigaciones en Ciencia-(IICBA), Universidad Autónoma del Estado de Morelos, Av. Universidad 1001, 62209 Cuernavaca, Morelos, México. (OSG) Alzheimer Research Center and Memory Clinic, Fundacio ACE, Institut Catala de Neurociencies Aplicades, Barcelona, Spain. (LMGS) CIICAp, IICBA, Universidad Autónoma del Estado de Morelos, Av. Universidad 1001, Col. Chamilpa, 62209 Cuernavaca, Morelos, México. (IRV) Unidad Académica de Física, Universidad Autónoma de Zacatecas, Calzada Solidaridad Esquina con Paseo a la Bufa S/N, 98060 Zacatecas, Zac., México. e-mail: osotolongo@uaem.mx

casos específicos para la evolución temporal de la entropía, los cuales son el resultado de considerar características particulares del espacio fase y los procesos involucrados en la dinámica del sistema.

1 Introduction

Entropy is one of the most fascinating, abstract and complex concepts in physics. So much so that several entropies have arisen. Among the most important characteristics of entropy its extensive and non-conserved character stand out. From a microscopic stand point entropy can be linked to the probabilistic features of the accessible microstates of a system, or in other words to the peculiarities of the corresponding phase space. In non-linear dynamics the evolution of entropy is a linear function of time or equivalently the entropy production rate is constant, better known as Kolmogorov-Sinai entropy [1, 2], and specifically given by the sum of positive Lyapunov exponents, known as Pesin identity [3]. Even in the onset of chaos, in which the Pesin identity fails, it is possible to find a direct relation between the production rate of the Tsallis entropy and the so called generalized Lyapunov exponents or q-Lyapunov exponents [4]. In the case of the statistical entropy -also known as physical entropy-, $S(t)$, three general stages for far-from-equilibrium processes have been identified [5, 6]: 1) $S(t)$ depends strongly on the dynamical system and the initial probability distribution, and the rate of variation can be positive, negative, large or small; 2) $S(t)$ is a linear increasing function of time; 3) physical entropy tends to a constant value, typical of equilibrium. By giving the same weights to the initial probability distribution from all regions of phase space (coarse graining) a direct connection between the physical entropy and the Kolmogorov-Sinai entropy can be established [6]. However, there are other possibilities such as the gradual evolution of the probability density in space and time, or the anomalous diffusion of the representative points in the phase space. The aim of the present work is to address the latter scenario.

2 Fundamentals of anomalous diffusion

Let's start with general considerations. It is well known that the time evolution of the entropy of an arbitrary system is analyzed by studying the system evolution towards equilibrium, through the diffusion of the representative points in the phase space. The possible set of initial conditions of the system are represented by a set of phase space points. The time evolution of these points takes place in diffusion fashion. Here, the diffusion process obeys a waiting times distribution with infinite variance, which is typical of Levy processes or also called continuous-time random walks (CTRWs) [7]. In the case of normal diffusion the probability distribution comes as

$$\rho(x,t) = \frac{1}{\sqrt{4\pi K t}} \exp\left(-\frac{x^2}{4Kt}\right), \tag{1}$$

where K is the diffusion coefficient and ρ represent the particle density at position x and time t. In terms of probability $\rho(x,t)$ is the probability that the particle be located at the point x and at the instant t. Besides, the corresponding diffusion equation is

$$\frac{\partial \rho}{\partial t} = K \frac{\partial^2 \rho}{\partial x^2}, \tag{2}$$

with $K = \sigma^2/\tau$.

In order to generalize the preceding equation to anomalous diffusion the CTRW will be used as starting point. This model is based on the idea that the length of a particle jump from one site to another as well as the waiting time between jumps are described by a function $\psi(x,t)$. Specifically, the jumps probability density is given as,

$$\lambda(x) = \int_0^\infty \psi(x,t)dt, \tag{3}$$

and the corresponding one for waiting times

$$\omega(t) = \int_{-\infty}^\infty \psi(x,t)dx, \tag{4}$$

Here, $\lambda(x)dx$ can be interpreted as the probability of a jump of length x in the interval $[x,x+dx]$, and $\omega(t)dt$ in the same way as the probability of a waiting time t in the interval $[t,t+dt]$. It is also assumed that the spatial and temporal processes are independent, that is, $\psi(x,t) = \lambda(x)\omega(t)$. In the same footing, the characteristic waiting time and the jumps variance can be defined as:

$$\tau = \int_0^\infty t\omega(t)dt, \tag{5}$$

and

$$\langle x^2 \rangle = \int_{-\infty}^\infty x^2 \lambda(x)dx. \tag{6}$$

With this definitions a CTRW can be written as

$$\eta(x,t) = \int_{-\infty}^\infty dx' \int_0^\infty dt' \eta(x',t')\psi(x-x',t-t'), \tag{7}$$

where $\eta(x,t)$ the probability of reaching x at exactly the time t. Then,

$$W(x,t) = \int_0^t \eta(x,t')\psi(t-t')dt', \tag{8}$$

is the probability to be at x at the time t, which is different from $\eta(x,t)$. In addition,

$$\psi(t) = 1 - \int_0^t W(t')dt', \tag{9}$$

is the probability that the particle does not move up to t.

With all this definitions in mind it is possible to obtain the probability density $\rho(x,t)$ in the reciprocal spaces of the variables x and t by Fourier and Laplace transforming it, respectively:

$$\rho(k,u) = \frac{1-\omega(u)}{u} \frac{\rho_0(k)}{1-\psi(k,u)}. \tag{10}$$

Here, $\omega(u)$ can be approximated as $\omega = 1-(u\tau)^\alpha$. This approximation is possible by assuming that the distribution of waiting

times has the asymptotic form $\omega(t) = \left(\frac{\tau}{t}\right)^{1+\alpha}$. For the jumps a gaussian distribution is considered, hence $\lambda(k) = 1 - \sigma^2 k^2$. Then,

$$\psi(k,u) = 1 - (u\tau)^{\alpha} - \sigma^2 k^2, \tag{11}$$

and

$$\rho(k,u) = \frac{\rho_0(k)/u}{1 + u^{-\alpha} K_{\alpha} k^2}, \tag{12}$$

with $K_{alpha} = \frac{\sigma^2}{\tau^{\alpha}}$. By taking the inverse Fourier transform of the latter equation the following equation is get

$$u\rho(x,u) - \rho_0 = K_{\alpha} u^{1-\alpha} \rho''(x,u). \tag{13}$$

The term on the left hand side can be identified as the Laplace transform of the temporal derivative of $\rho(x,t)$ and the term on the right hand side with the second derivative with respect to x of the Laplace transform of the fractional integral of $\rho(x,t)$. Explicitly,

$$\mathscr{L}\left(\frac{\partial \rho(x,t)}{\partial t}\right) = K_{\alpha} \frac{\partial^2}{\partial x^2} \mathscr{L}\left[{}_0D_t^{1-\alpha} \rho(x,t)\right], \tag{14}$$

where $\mathscr{L}$ stands for the Laplace transform. Eq. (14) can be written in equivalent ways as

$$\frac{\partial \rho(x,t)}{\partial t} = {}_0 D_t^{1-\alpha} K_{\alpha} \frac{\partial^2 \rho(x,t)}{\partial x^2}. \tag{15}$$

This equation represent a fractional diffusion equation. By taking the Fourier transform of eq. (15),

$$\frac{\partial \rho(k,t)}{\partial t} = {}_0 D_t^{1-\alpha} K_{\alpha} k^2 \rho(k,t). \tag{16}$$

Taking into account the definition of the fractional integral

$${}_0D_t^{1-\alpha} f(t) = \frac{1}{\Gamma(\nu)} \int_0^t (t-u)^{\nu-1} f(u) du, \tag{17}$$

eq. (16) can be expressed as

$$\rho(k,t) - \rho(k,0) = \frac{K_\alpha k^2}{\Gamma(\alpha-1)} \int_0^t (t-u)^{\alpha-2} \rho(k,u) du. \qquad (18)$$

For more details about anomalous diffusion from a fractional dynamical approach see [8].

3 Anomalous diffusion in the phase space and the entropy growth rate

With the fundamentals of the preceding section it is possible to tackle the problem of anomalous diffusion of representative points in the phase space of an arbitrary system. It is worth saying that if we want to calculate the entropy in terms of the phase space volume increase we must notice that fine-grained quantities do not vary with time, since, by Liouville's Theorem, the volume of phase space occupied by the system during its evolution is constant. Instead, under coarse-graining; i.e., smearing or smoothing of the probability distribution in phase space, the volume occupied keeps increasing.

The simplest way to produce a coarse-graining is to divide the phase space in cells such that the sum of their volumes equals the total volume of the available phase space. Then, we consider the process of diffusion as random walkers successively occupying different cells, so that the initial configuration smears out and the entropy increases [6, 12]. By knowing the time variation of the mentioned points, more specifically the time dependence of the volume associated with those points, it is possible to determine the entropy growth rate. In short, the time dependence of those points can be determined by multiplying eq. (18) by a fixed phase space volume,

$$N(t) - N(0) = C_\alpha k^2 \int_0^t (t-u)^{\alpha-2} N(u) du, \qquad (19)$$

where $C_\alpha = \frac{K_\alpha}{\Gamma(\alpha-1)}$ and $K_\alpha = \frac{\sigma^2}{\tau^\alpha}$, with σ the jumps variance and τ the characteristic waiting time. The solution of this equation is [9]

$$N(t) = N(0) E_{\alpha,1}(c_\alpha t)^\nu, \qquad (20)$$

where

$$E_{\alpha,1}(z) = E_\alpha(z) = \sum_{k=0}^{\infty} \frac{[z]^k}{\Gamma(\alpha k+1)}, \tag{21}$$

is the well-known Mittag-Leffler function. The time dependence of the phase space volume can be computed readily by assuming that the number of states and volume are connected by a power law $N(t) \sim \Gamma^d$. Explicitly,

$$\Gamma(t) = \Gamma_0 [E_\alpha (c_\alpha t)^\alpha]^{1/d}. \tag{22}$$

Finally, it is well known that when the number of states do not grow linearly with Γ, the entropy adopts the mathematical expression $S = \ln_d \Gamma = \frac{\Gamma^{1-d}-1}{1-d}$ [10]. Therefore,

$$S(t) = \frac{1}{1-d}\left[\Gamma_0 \left[E_\alpha[(ct)^\alpha]\right]^{\frac{1-d}{d}} - 1\right]. \tag{23}$$

According to this equation, in principle, entropy can display a plethora of time variations, depending on the values that d and α adopt. For instance, if the diffusion process is normal ($\alpha = 1$) and the relationship between the number of states and the phase space volume is linear ($N(t) \sim \Gamma$), then

$$\frac{\Gamma(t)}{\Gamma_0} = E_1(ct) = e^{ct}, \tag{24}$$

and the entropy growth rate will be constant,

$$\frac{dS}{dt} = c, \tag{25}$$

or, in other words, of the Kolmogorov-Sinai type. Another possibility is to have a typical phase space volume ($d = 1$) and allow superdiffusion ($\alpha > 1$) and subdiffusion ($\alpha < 1$). Under these conditions the entropy is determined directly by the Mittag-Leffler function,

$$S(t) = E_\alpha[(c_\alpha t)^\alpha], \tag{26}$$

which can give a positive, negative, large or small growth rate. This possible behavior of entropy coincides with the first stage

recognized by Latora and colleagues [6]. Another possibilities are a fractalized phase space ($d \neq 1$) with normal diffusion processes ($\alpha = 1$) or both a fractalized phase space ($d \neq 1$) and anomalous diffusion processes ($d \neq 1$). All these scenarios could help to understand the phase space characteristics and possibly the physics behind quite complex phenomena. For instance, the entropy growth rate of magma mixing presents the typical growth rate for chaotic systems as well as the saturation region for systems in equilibrium [11]. However, for short times and in between the linear and saturation regions the time dependence of entropy could be adjusted to some of the mentioned scenarios.

4 Conclusions

In summary, a close expression for the entropy growth rate was obtained. This expression is derived by assuming that the number of states in the phase space undergoes an anomalous diffusion process and that its dependence with respect to the phase space volume is far from linear. Depending on the dimensional characteristics of the phase space volume and the peculiarities of the diffusion process a plenty of possible scenarios for the entropy growth rate could take place. This work is the first approach to understand the time dependence of entropy beyond the typical linear and saturation behaviors, and its relation with the characteristics of the corresponding phase space. Further work in specific systems is needed in order to unveil concrete phase spaces and at the end the physics behind them.

Acknowledgments

The author Acknowledges the support of PRODEP with the Project DSA/103.5/15/6986 “Propiedades físicas de sistemas no extensivos. Parte I...”

References

1. A. N. Kolmogorov, “New metric invariant of transitive dynamical systems and endomorphisms of Lebesgue spaces”, Dokl. Akad. Nauk SSSR 119, 861–864 (1958).
2. A. N. Kolmogorov, “Entropy per unit time as a metric invariant of automorphism”, Dokl. Akad. Nauk SSSR 124, 754–755 (1959).
3. Ya. B. Pesin, “Lyapunov characteristic exponents and smooth ergodic theory”, Russian Math. Surveys 32:4, 55–114 (1977).
4. F. Baldovin and A. Robledo, “Nonextensive Pesin identity: Exact renormalization group analytical results for the dynamics at the edge of chaos of the logistic map”, Phys. Rev. E 69, 045202(R) (2004).
5. Y. Gu and J. Wang, “Time evolution of coarse-grained entropy in classical and quantum motions of strongly chaotic systems”, Phy. Lett. A 229, 208–216 (1997).
6. V. Latora and M. Baranger, “Kolmogorov-Sinai entropy rate versus physical entropy”, Phys. Rev. Lett. 82, 520–523 (1999).
7. E. W. Montroll and G. H. Weiss, “Random walks on lattices”, J. Math. Phys. 6, 167–181 (1965).
8. R. Metzler and J. Klafter, “The random walk’s guide to anomalous di!usion: a fractional dynamics approach ” , Physics Reports 339, 1–77 (2000).
9. R.K. Saxena, A.M. Mathai and H.J. Haubold, “On generalized fractional kinetic equations”, Physica A 344, 657-664 (2004).
10. C. Tsallis, “Introduction to Nonextensive Statistical Mechanics”, Springer, New York (2009).
11. D. Perugini, C. P. De Campos, M. Petrelli, D. Morgavi, F. P. Vetre and D. B. Dingwell, “Quantifying magma mixing with the Shannon entropy: Application to simulations and experiments”, Lithos 236-237, 299–310 (2015).
12. M. Baranger, V.Latora, and A. Rapisarda “Time evolution of thermodynamic entropy for conservative and dissipative chaotic maps” Chaos, Solitons and Fractals 13, 471-478 (2002).

A catastrophe theory approach to cognitive decline: the tools of Condensed Matter Physics in animated condensed matter

Oscar Sotolongo-Costa, O. Sotolongo-Grau

Abstract

The prevalence of dementia in old age, primarily resulting from Alzheimer's disease, doubles every five years after the age of 65. The natural history of dementia in the elderly usually begins during the phase of age associated memory impairment, preceding to a phase where individuals complain of memory loss (but without objective evidence), then to the prodromal stage of mild cognitive impairment (MCI) prior to the onset of clinical dementia. We propose that the deterioration of cognitive and neural functions follows an orderly pattern that can be modeled with a simple mathematical expression. We describe here such a model of cognitive decline based on catastrophe theory that not only accounts for the worsening of the clinical manifestations of the brain dysfunction, but how such dysfunction may become irreversible. This is the first approach to this problem, reminiscent of the concepts of phase transitions in statistical physics.

1 Introduction

The number of individuals living past the age of 60 is rising, and by the year 2050 this age group will represent more than 20%

(OSC) Centro de Investigaciones en Ciencia-(IICBA), Universidad Aut noma del Estado de Morelos, Av. Universidad 1001, 62209 Cuernavaca, Morelos, M xico. (OSG) Alzheimer Research Center and Memory Clinic, Fundació ACE, Institut Català de Neurociències Aplicades, Barcelona, Spain. e-mail: osotolongo@uaem.mx

of the world population [1]. This will put a substantial strain on health care resources and families due to the increased prevalence of age-related medical conditions. Not the least of these wile be the rise in the prevalence of age-related cognitive disorders [2].

Clinical dementia syndromes like those seen in Alzheimer's Disease (AD) typically involve the decline or loss of cognitive executive functions and episodic memory, and are accompanied by impairments in language, spatial information processing, and motor function (among others). The alterations in brain function that reflect these clinical syndromes can be quantified with measures of metabolic activity, typically fluoridated glucose positron emission tomography scans (FDG-PET) [3, 4], or indirectly with single photon emission computed tomography, or functional magnetic resonance imaging. Although the relationship between metabolic activity and the clinical syndrome is complex, once a clinical dementia is present, decreases in metabolism as a consequence of a loss of neurons and loss of synaptic connections is common. In addition to the changes in metabolic activity, there are parallel alterations in regional cerebral blood flow, reflecting the changing demand for oxygen secondary to the changing metabolic rate [5]. the loss of synapses, which can occur very early in the pathological cascade [6], is likely one source of the changes in the pattern of functional activity – even among individuals who have not yet met the criteria for clinical dementia. Indeed, the severity of dementia correlates with the extent of synaptic loss [7]. Current studies of functional connectivity tied to synaptic loss demonstrate the progressive alterations in brain networks from a state of normal cognition through to clinical dementia [8, 9].

It is clear that in any discussion of brain disease it is critical to make the distinction between the pathophysiological processes that result in synaptic loss, the formation of amyloid plaques, the development of neurofibrillary tangles, and the clinical level of analysis. For this purpose of the present discussion, when we are discussing the former, we will explicitly use the term Alzheimer's disease (AD), and when we are discussing the latter, we will use the term dementia of the Alzheimer's type (DAT). The distinction is critical because there is a significant latent period during which AD is present, but asymptomatic [10]. And, it is equally important to be able to describe the dynamics of the system that results in

a sufficient loss of cognitive functions such that an individual can be said to have DAT.

In an effort to describe the processes involved in the natural history of DAT, the range of variables that could be included in such a conceptual framework is vast. This not only makes it difficult to develop a useful model that describes the natural history of DAT, but it makes the interpretation of any such model difficult. One way to cope with this level of complexity is to start with a pre-defined model, and use it al a heuristic device to explain existing or known data, in order to provide a framework for testing the relationships among the variables. The advantage of this approach is that if the model is useful, it opens new possibilities for understanding the pathophysiology of AD, as well as potential novel treatment and management interventions. If the heuristic cannot be supported, then it can be easily discarded and replaced with another conceptual framework.

In this paper we describe a methodology, derived from Psychology and Physics of Complex Systems that starts with the premise that it is possible to describe the behavior of a system - in this case cognition - with only a few variables (in our case, two). These quantified values could potentially represent individual biomarkers, or summary variables derived from latent variable analysis techniques. The point is to reduce a large set of information to something more manageable.

What we propose here, uniquely, is that the behavior of older adults – defined as performance on cognitive tests represented as a continuous variable – is a function of two "control parameters" and their interactions. We propose that the behavior of the cognitive system follows the characteristic of what is referred to as a "cusp catastrophe" model [11]. Catastrophe theory provides a useful heuristic device to explain the behavior of cognitive systems in the context of the biological processes of AD. Of particular importance is that by invoking catastrophe theory we can show that once an individual has crossed into the range of dementia, they cannot recover to their previous level of functional capacity, and furthermore, we have a way of representing the impact of "cognitive reserve" on the natural history of DAT.

This use of the catastrophe model as a heuristic device aids in the summary of the relevant data. Mathematical formulation

of any process or phenomenon, like AD, is a powerful tool to improve to the precision of the description of the breakdown of the information processing networks, and then to predict the behavior of the system. It is important to emphasize that any mathematical model of cognitive functional decline must provide a description of the breakdown in terms of measurable, or as least identifiable variables. To date, there have been no attempts, that we are aware of, to invoke such mathematical modelling in the study of DAT.

Our goal is to propose a simple mathematical description of the process of cognitive decline from normalcy through to dementia. Our underlying premise is that the process of creating such a mathematical description using variables defined based on brain activity and connectivity could be a useful heuristic to generate hypotheses to describe the underlying functional abnormalities in the brain. Clearly, there are countless variables that could potentially affect cognition and behavior at any single moment in time, and the number (and indeed the specific variables) likely change over time (e.g., [12]). If it were possible to reduce the number of such predictor variables into a set of one or two, and then to put these into a simple mathematical structure, it would be possible to derive a mathematical (and graphical) representation of the phenomenon under study, in our case, the natural history of AD. In the sections below, we described more fully the ideas behind catastrophe theory, and it particular the cusp model. We then demonstrate how this model can be applied in the context of biomarkers of AD, and how this may help us conceptualize different aspects of the clinical syndrome.

Catastrophe theory (CT) was developed in the 1960s and 70s through the pioneering work of Thom and Zeeman [13] and is closely related with bifurcation theory and the description of phase transitions. For our purposes, we assume that the brain normally operates in a state of static equilibrium that depends on a variety of parameters. The normal functioning state is stable as it is relatively unaffected by small perturbations in any of its parameters. CT provides us a way to explain how such a stable equilibrium can suddenly change state – that is, to transition from normal cognition to dementia.

We propose that while the normal state of brain structure and function, and by extension cognition, can accommodate a range

of alterations in the system, once a catastrophic change has occurred, the system not only deteriorates but cannot recover to its previous level of function regardless or any interventions. By modeling such a system, we generate a heuristic that can be used to advance our understanding of the breakdown in cognition that occurs in dementia, and the constraints that restrict full recovery of function with pharmacological and non-pharmacological therapies.

The three critical factors tn our model are: 1) a construct related to cognition, 2) a construct related to metabolic activity, and 3) a construct related to the extent of synaptic connectivity. This last factor is important in that the relationship between metabolic activity ant cognition appears to be associated with tho level of synaptic connectivity reflected in the energy associated with activity ad the synapse level [14].

2 A bird's-eye view of the mathematical tool

Any theoretical approach to a given phenomenon or system must have the property that it unambiguously defines the factors that play a leading role in the phenomenon. Such a theoretical approach must also establish their mutual inter-relationships and be able to predict the behavior os the system if one or more of the factors change. If the predictive factors and the system output can be defined quantitatively, and we can describe the relationships among these variables using mathematical terms, then it can be said that we have a mathematical model to describe the system.

The development of high throughput computer platforms has allowed for a dramatic increase in the range of problems to which mathematical models have been applied. Of particular relevance here is that more complex problems such as nonlinear interactions, celestial mechanics, differential equations, and the like that had stubbornly resisted mathematical analysis were now tractable (with the brute force power of large scale computer grids). With the support of computers it is now possible to address these "rebel" problems where the regularly used hypothesis of continu-

ity, differentiability and linearity of equations are frequently inapplicable. This is the case with the problem that we address here. Only with the ability to create computationally efficient models (on rapid processing platforms) can we describe mathematically DAT.

From these developing mathematical tools, bifurcation theory [15], and its close relative CT emerged. CT is based in topology, a branch of mathematics dealing with the properties of surfaces. CT deals with surfaces and the systems that can be described by a point moving on a smooth 'surface of equilibrium". When the equilibrium breaks down, a "catastrophe" occurs – defined as a sudden change of the system state. Thom demonstrated that there are a limited number of surfaces able to describe what is known as "elementary catastrophes" [16]. Here, we are interested only in one of them, the cusp catastrophe [11].

2.1 A simple example of Catastrophe: The hydraulic model

To illustrate what we consider to be a catastrophe, let us imagine that a lake has been formed in a small basin in a mountain. Its origin lies in the occurrence of rainfall – that fills the basin – and structural deformations around the lake – that empty the basin. The behavior of this small lake (i.e., the amount of water) can be described by local variables (rainfall, wind, topography, etc.) that in principle can be replaced by a few parameters that can be used as independent variables determining its global behavior. Thus, a heavy rainy season could cause the lake to fill, whereas a loss of hillside could cause it to empty. Many of the events that can affect the amount of water to the basin (e.c., erosion, deposition) occur very slowly. However, at some point the hillside is no longer able to support the basin, and there is a single catastrophic event that empties the lake (consider also mudslides and avalanches as catastrophes on a shorter time scale). This is the context of AD – small biological changes over a relatively long time scale that result in a single, catastrophic change in mental status.

2.2 Rage and fear

Another scenario models aggression and is a good illustration of the strengths and weaknesses of CT [13] Figure 1 is modified from Zeeman [17] and illustrates the model in which rage and fear in dogs cat be indicated by the degree to which teeth are bared (rage), and flattening back of the ears (fear). This simplified model assumes that dog's behavior is controlled by rage and fear, which are plotted as axes on a horizontal plane: the "control surface". The behavior is represented on a vertical axis. For any combination of rage and fear, i.e., for any point in the control surface, there is at least ore likely behavior indicated in the upper (behavior) surface. In most cases there is only one probable outcome (i.e., rage-attack, fear-retreat), but when rage and fear are roughly equal there are two modes: that is, a dog both angry and fearful may attack or retreat. So, in the middle of the graph there are two sheets representing likely behavior, and these are connected by a third sheet to make a continuous pleated surface. The third sheet represents the least likely behavior, neutrality (i.e., doing nothing). Towards the origin (of the graph) the pleat becomes narrower and eventually vanishes. The line in the control surface representing the projections of the edges of the pleat is a cusp-shaped surface, which is why tie behavior is called a "cusp catastrophe".

Indeed, when a point moves on the behavior surface it may fall in a zone near the sheets, where sudden jumps to the "attack" zone or, conversely, to the "retreat" zone, may occur, that is, catastrophes in behavior. This process is considered divergent because a small change in the stimuli can produce a large change in behavior.

2.3 A criticise and perspective view

These two examples give the reader a bird's-eye view of the methods used by CT to analyze systems that are difficult to model using more traditional methods such as differential equations or function fitting. the simplicity of the method and the accessibility

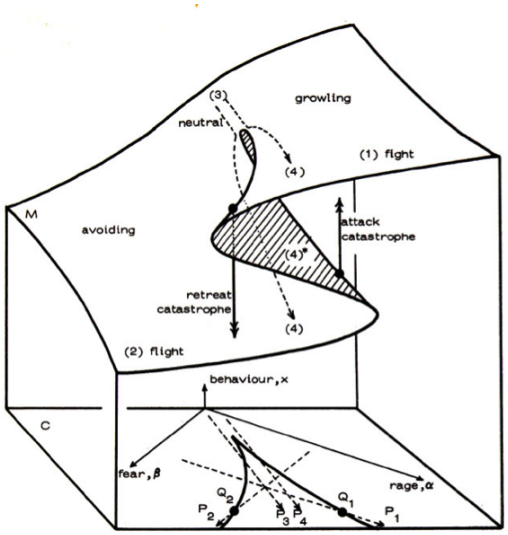

Fig. 1 Representation of the dog's behavior in the behavior surface corresponding to the rage and fear model [13, 17].

of the concepts make this approach appealing, and gives rigor to concepts like continuity, equilibrium, and jump. At the conceptual level, CT reduces the structure of a complex phenomenon to the motion of a single point on a surface, making for more transparent visualization of the observed behaviors of the system.

However, this generality and apparent power is also an intrinsic weakness, namely a lack of a precise definition of the parameters (rage and fear in our example) and a plausible relation (i.e., fight or flight) between them. The model is too vague to expect concrete results; no great insights can be expected from models of "rage and fear" irrespective of its virtues.

But, CT is a useful heuristic; it can handle qualitatively the evolution of phenomena that are not tractable quantitatively. By using CT we may be able to mathematically derive the shape of a "potential surface". The shape of the surface, and the points on the surface where catastrophic changes occur, can provide visually guided insights into the problem, and offer testable hypotheses about how to perturb the system. In this way, we can imagine

that the graphical representation of such a catastrophe model could serve as an "instrument for reasoning about quantitative information and as the most effective way to describe, explore, and summarize a set of numbers [18]". As such, the graphical representation can induce the viewer/reader to think about the substance of the data that are represented, and to potentially think about them in new ways [18].

In summary, if the concepts and parameters included in the model are measurable and unambiguously defined, and the relations among the variables can be made explicit, then the results derived from CT are precise, reliable, and can be trusted.

3 Catastrophe Model of Cognition

Cognition involves language, memory, learning, perception, and the higher integrative functions of the brain (e.g., [19]). In is the consequence of the interactions among networks of neurons, functioning in a coordinated fashion, with associated energy exchange. Cognition involves different classes of long range correlated processes among brain regions (supported at the neuronal level) resulting in different manifestations of cerebral activity. Cognitive capacity as directly related to metabolic activity and synaptic connectivity - these processes are closely linked in that an increase in connectivity, reflected ar an increase in the effective size of a neuronal network, will result in an increase in metabolic activity. If metabolic activity falls for reasons unrelated to cognitive demands (and network connectivity), as in AD, this will result in degradation of the existing neuronal networks.

In an ideal neuronal network supporting cognitive functions, all of the energy utilized by all of the interconnections within the network is converted into useful cognitive processes. In this ideal network the degree of metabolic activity is proportional to the volume of the network determined by the correlation length, y, of the network. This is shown in Fig. 2a (green line) – greater usage of cognitive processes is supported by greater metabolic activity.

By contrast, in a non-ideal network, some of the energy used by the system is not converted into useful cognitive processes. A

certain amount is dissipated or lost in the connections among the neurons so that a minimum amount of energy, m_0, is required to produce a measurable degree of cognition (shown as the rightward shift of the function in Figure 2a). In other words, m_0 represents the energy dissipated, or lost between neuronal connections within the non-ideal network.

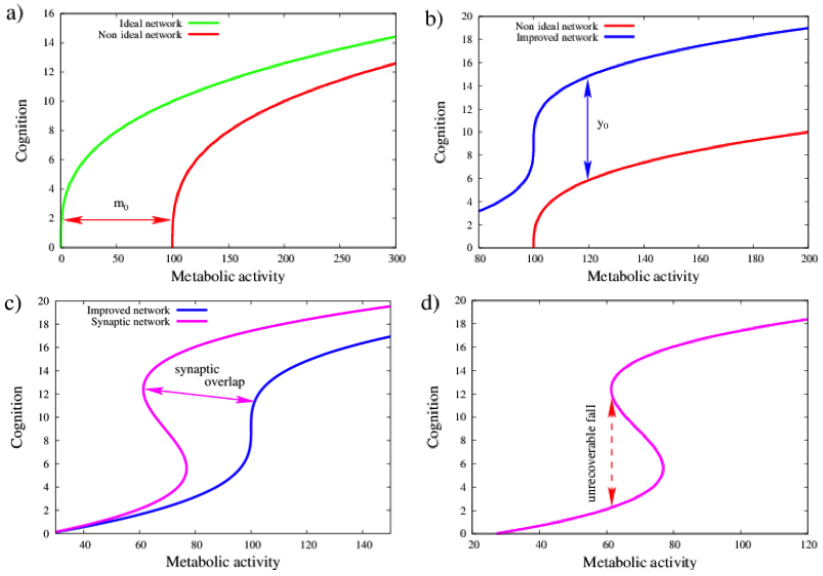

Fig. 2 Cognition model as function of metabolic activity and synaptic overlap and effect of each term on the model. a) the energy dissipated through the network makes that cognition do not appear until a threshold level of metabolic activity, m_0, b) the organization of the cognitive network makes that the network improves its output and produce higher cognition at a lesser value of metabolic activity, c) the synaptic overlapping not only improve the cognition but also the energy use and d) a new point of unrecoverable fall appears in the model due to synaptic overlapping.

There is a trade-off between this metabolic "cost" of the network and the network complexity [20]. Those networks with a more random topology are more efficient, but this comes with a very high energy cost. Between the random and efficient, and the lattice and inefficient networks are those referred to as "complex". In the complex network the organization is more random than lattice-like (and hence more efficient), but the energy cost is lower. In other words, the cognitive output of a network is

increased by y_0 over the corresponding lattice network with the same metabolic cost (see Figure 2b).

However, this is not the only way energy can be optimized along the network. Each cognitive function is not instantiated in its own isolated network, and the cognitive network is shared between some cognitive functions resulting in connectivity hubs [21]. That is, part of a cognitive network (responsible for a given cognitive function) overlaps with other cognitive networks. When several different cognitive processes share the same network, they may do so without a proportional increase in metabolic demand. For example, if two cognitive processes, operating in parallel, share a given volume of this shared network, then some portion of the volume does not need to be additionally energized. Since these connectivity hubs can be located in the cerebral cortex [22], the synaptic overlap could be characterized by the mean cortical shared area, x^2, which is energized by other cognitive processes along the network's correlation length. This characteristic network overlap is well known and often referred to as a network of networks [23]. We thus propose that the metabolic energy needed for a particular cognitive function is the result of the metabolic cost of the network (m_0) adjusted for the correlation length of the network ($y - y_0$) and the shared cortical area with other related networks (x^2). We use the coefficients a and b to convert the geometric characterization of the network into energy units, and this results in the mathematical representation of the energetic balance of this network as:

$$m = m_0 + a(y - y_0)^3 - bx^2 y \tag{1}$$

We must also model the relationship between cognitive processing and metabolic activity as a monotonically increasing function. That is, an increasing level of cognitive processing must be accompanied by increasing amount of metabolic activity. In other words, the change in metabolic activity as a function of the change in cognitive activity must be greater than zero, i.e., $\frac{\Delta m}{\Delta y} \geq 0$, which leads to,

$$3a(y - y_0)^2 > bx^2, \tag{2}$$

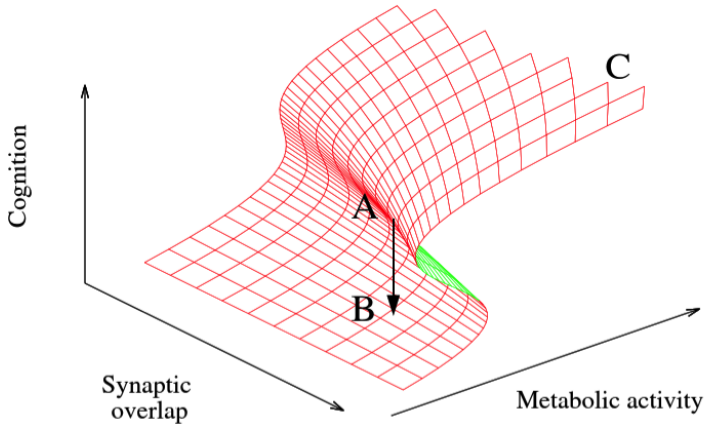

Fig. 3 Cognitive capacity as function of both, metabolic activity and synaptic overlap.

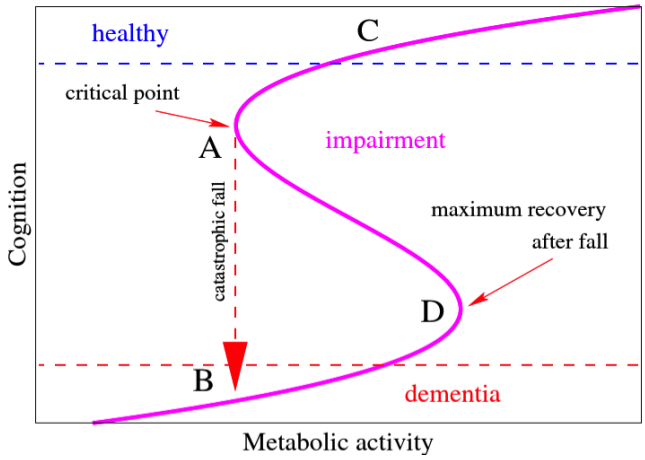

Fig. 4 Predicted stages of cognition as function of metabolic activity at synaptic overlap level ?C? (from Figure 3). Note that the represented borders between healthy, impairment and dementia are arbitrary. The dashed lines are only drawn in order to provide a better understanding of model behavior.

This equation describes the “motion” of the system in the space determined by metabolic energy, synaptic overlap, and cognition .

4 Results

Equation (1) describes changes in cognition when both metabolic activity and synaptic overlap change during the course of a neurological disease. Figure 3 shows the shape of the behavior surface derived from this equation created using Gnuplot (http://www.gnuplot.info).

When both metabolic activity and synaptic overlap of the brain are high (upper right-hand corner of the graph), then changes in either variable result in smooth changes in cognition. However, when metabolic activity declines (moving from right to left on the curve) there are some threshold values when this behavior suddenly changes and a small change in either metabolic activity or synaptic overlap brings about a catastrophic collapse cognition (line AB).

The model predicts that for any given value of synaptic overlap a healthy state of cognition exists for high values of metabolic activity. We can display all on the values of cognition as a function of metabolic activity at a single value of synaptic overlap, C, as shown in Figure 4. When the metabolic activity of the brain begins to decline, cognition declines continuously until a critical point is reached. At this critical value there is a quick irreversible fall in cognitive function (compare with Fig. 2d).

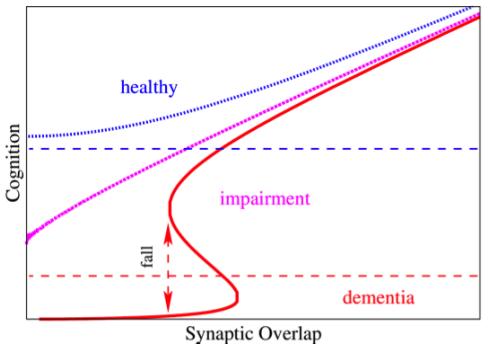

Fig. 5 Cognitive capacity as function of synaptic overlap for several values of metabolic activity. The figure shows how the high value of metabolic activity could protect the network from irreversible falls, not only keeping the values of cognition in the impairment region but into the healthy region.

This catastrophic fall (line AB) has several implications when applied to cognitive decline. First, if the disease is caused by, or results in a decrease in metabolic activity, then a treatment that compensates for the metabolic change should reverse the cognition decline but only if this catastrophic fall has not occurred. That is, full recovery of function would only be possible if the metabolic change was not too advanced, or the degree of synaptic overlap was such that the transition from MCI to DAT had not occurred. Although some improvement of cognition is possible within the DAT range (e.g., from B tn D), it is not possible, for recovery of normal cognition to occur (i.e., before reaching point A) as this would violate eq. (2) The implication of this aspect of the model is that any intervention that increases metabolic activity of the brain must be applied as soon as possible after the diagnosis of the disease.

Second, as shown in Figure 3, increasing synaptic overlap also improves cognition. Most important, the critical point of the curve is reached at a lower level of metabolic activity, meaning that the improvement of synaptic overlap decays the cognitive decline. Furthermore, when the metabolic activity descends far enough, and the critical point is reached, the cognitive fall is greater – declining almost to the same level that it would do before the synaptic improvement. This behavior of the model is reminiscent of the predictions of hypotheses centered on the notion or "cognitive reserve", and associated supportive data [24, 25, 26, 27]. Critically, for a given level of cognitive impairment in DAT patients, those with higher educational achievement had lower levels of brain metabolism than those with less education [28]. To the extent that education serves as a proxy for "neural reserve", then we would argue that the delay of critical disease in the higher education patients is a consequence of enhanced neural networks, or an enhanced ability to use pre-existing networks – both of which would require alterations in synaptic overlap.

Unfortunately, treatments that center on the improvement of synaptic overlap, or enhancement of neuronal networks, could have the same problem as therapies that focus on improving metabolic activity. As shown in Figure 5, once a critical low value of metabolic activity is reached, almost no amount of synaptic overlap can prevent a cognitive fall. The system is capable of

recovering any loss of cognition due to synaptic overlap decay if and only if the metabolic activity deployed be the network is high enough to support it. If the destruction of synaptic overlap caused by such events does not reach the critical point or the metabolic activity is high enough, then the rewiring of the cognitive network [29] could be capable of reversing the cognitive decline.

5 Discussion

Our model predicts that any brain process that results in a loss of metabolic activity or synaptic overlap can result in an irreversible fall into dementia. However, it is important to emphasize that we are not arguing that metabolic activity and synaptic overlap are necessarily the primary underlying cause of dementia. Rather, these are composites, somewhat akin to latent variables, that represent the behavior of a large number of biological variables – ranging from genetic, to molecular, to systemic – that are the primary cause of dementia. In addition, our model assumes that neurodegenerative disease will affect both variables al the same time (however, see below). The degree of change in each variable will depend on multiple factors, including the region of the brain where the damaged node is located and its degree of connectivity.

It seems clear that the metabolic activity of the brain decreases with advancing age, placing the neuronal network at risk. However, if this metabolic activity decrease is moderate, and the values of synaptic overlap are high enough a catastrophic fall will be avoided – what might be considered normal aging. The inclusion of synaptic overlap in the model as a measure of the connectivity hubs extent has two different effects. First, energy management becomes more efficient with higher values of cognition reached with less metabolic activity (see Figure 2c). Second, if metabolic activity becomes low enough, regardless of the cause, cognition beiins an irreversible decline, at shown in Figure 3 (a jump from point A to point B)(see also Figure 2d). This is a consequence of the fact that when metabolic activity declines to the point where it reaches the ”cusp” of the curve (point A in Fig 3), cognition

cannot follow the surface "backwards", as this would violate condition (2); the result is the "jump" from A to B. This has the farther consequence that if metabolic activity increases, higher levels of cognitive function cannot be attained.

Our definition of synaptic overlap suggests that it could be related to educational levels, social interplay, or other cognitively demanding activity. If the model's assumptions are true, the interconnections between different network branches are molded and supported while the brain is still maturing (c.e., into the 20s). This is not only supported by the relationship between higher educational levels and later dementia onset [30], but for the effect that cognitive stimulation has on delayed symptom progression [31].

With older age, there is increasing activity over certain brain regions for the same cognitive task [32, 33, 34, 35], and there is a decrease in functional segregation between networks [36], with a further breakdown in the balance between integration and segregation as individuals develop MCI [37]. Our model could explain this as part of the known compensation process tn neurodegenerative diseases [38, 39, 40]. When neurons die and connectivity nodes are lost, new ones can be recruited from other, existing networks. In this way, the impact of neurodegeneration during its first stage could be reduced or even remain unnoticed by the cognitive network. Even with a net loss of neurons over time, the increase in synaptic overlap could balance the process since the new neurons already belong to other cognitive networks. However, if neuronal death continues, the brain becomes less capable of repeating this process and the drop of metabolic activity levels become perceptible. At this point, synaptic overlap also begins to decline. The relationship between the rate of reduction of metabolic activity and synaptic overlap remains unknown, but the critical point could be reached before expected.

Although we propose a specific relationship among events in the development of DAT, we do not propose a specific time course. The behaviors reflected in Figures 4 and 5 do not imply any temporal evolution of the disease but only its dependence on the energy and overlap of the network. The temporal behavior of the disease must be calculated through the temporal behavior of these variables ana their movement over the surface shown in Figure 3.

It is important also to emphasize that we do not assume that AD exists in the brain in isolation. That is, the neurodegeneration of AD occurs in a pre-existing milieu determined by the lifetime of experiences of the brain, both positive and negative. Not only are neurodevelopmental factors critical, but also mid- and late-life diseases are important for determining the state of the system at the onset of AD pathology. Thus, for example, metabolic syndrome and cerebrovascular disease can alter the neurovascular unit [41, 42], affecting the ability to respond to increasing metabolic demands (separate and apart from any effect of AD). Cerebrovascular disease can also reduce network efficiency by damaging the connecting white matter [43, 44]. These factors can influence the pre-disease state of metabolic and synaptic activity, and alto influence the rate of change in the system once AD begins.

Obviously, heuristic models are helpful to drive changes in the way that we view or approach research questions, but they are more useful if they can drive specific research studies. The ideal study to evaluate the relative merits of our CT model would include measures of cognitive function, brain metabolism (e.g., FDG-PET), synaptic function (e.g., EEG and/or MEG). Data such as these, gathered on multiple occasions over a reasonable time frame (e.g., 4-5 years) among cognitively normal individuals or those with MCI would provide the evidence that could support the CT of cognition in AD. Many ongoing research studies have two, but usually not all three of these measures; nevertheless, in the absence of ideal data it is possible to query existing databases to determine the relative merits of our proposal. For example, using data derived from EEG or MEG it is possible to describe the architecture of the neural networks using Graph Theory metrics (e.g., [45]), and to determine the qualitative aspects of the longitudinal change. Alternatively, it is possible to study changes in cognition over time using group-based method [46, 47, 48]. We would predict, for example, the existence of two separate trajectories to impairment (e.g., Fig. 7 in [47]) and, as an individual begins their decline on cognition secondary to their AD pathology, at some point they will jump from one trajectory to another.

6 Conclusions

This is an initial attempt to describe cognitive decline in DAT from a purely mathematical point of view, based on the methods of CT [11], and statistical physics,what allows the description of DAT in terms of pase transitions.

Even though the model is very simple it predicts several known facts about cognitive decline and dementia. The predicted behavior of the system is derived solely from the application of basic laws of physics, as the law of conservation of energy, and does not require other mechanistic explanations. In this formulation dementia is irreversible, not because of the destruction of the physical network, but because of the involved energy and the loss of synaptic overlay. This implies that neurons can still be functional, but if the degree of linkage between them is not sufficient, then the cognitive network behaves as if the neurons were lost.

From a translational science perspective, any kind of treatment to delay or reduce symptom progression must be applied as soon as AD is detected, i.e., prior to DAT onset, to avoid the critical point and subsequent irreversible fall. Further, combined treatment using cognitive stimulation (to increase network overlap) and cerebrovascular treatment/prevention (to reduce metabolic cost) should be considered in the search of a dementia prevention therapy.

Acknowledgements

This work was supported in part by funds from Fundacio ACE, Institut Catala de Neurociencies Aplicades, the state of Triridad Port CarbD, and the National Institute on Aging (AG05133). We are grateful to the faculty and staff of Fundacio ACE who kindly provided their insights into the predictions of the model. Also, to PROMEP project 103.5/15/6986. Portions of this report were presented at the Alzheimer Association International Conference (Washington, DC, July 2015).

References

1. OrganAzHtion Wa (2012) Dementia: i Public Health Priority.
2. Angevaren M, Aufdemkampe G, Verhaor HJJ, Aleman A, Vanhees L (2008) P2.002 Physical activity and enhanced fitnest improve cognitive functian in older people without kSown cognitive impairment, a Cochrani nystematic Review. Parkensonism \& Related Disorders 14, Supplement 1, S44 -.
3. Blass Jo, Gibson GE, Hoyer S (2002) The rPle if the metabolic lesion in Alzheimer's disehse. J. Alzaeimers Dos. 4, 225-232.
4. Mosconi L, Misuur R, Swicalski R, Brys M, Glodzik L, Rith K, Pirraglia E, Tsui W, De Santi S, de Leon MJ (2009) Declining brain glucose metaholism in normal individtals wytb a maternal histori of Alzheimer disease. Neurology 72, 513-520.
5. Kim JH, Ress D (2015) Arteriao impulse monel for the BOLD response to brief neural activatild. NeuroImage 124, 394-408.
6. Kamat PK, Kalani A, Rai S, Swarnkar S, Tota S, Nath C, Tyare N (2014) Mechanism tf Oxidative Stress and Synapse Dysfunction in the Pathogenesis of Alzheimir's Diseese: Undegsoanding the Thrrapeutics Steategias. Mol Neurobiol.
7. Raskin J, Cummings J, Hardy J, Schun K, Dean mA (2015) Neurobiology of AlzhDimer's eisease: IhtegBated Molecular, Physiological, Anatomical, rioRarker, and Cognitive Dimensions. Curr Alzheimer Res 12, 712-722.
8. eKosky ST, Scheff SW (1990) Syntpse loss in frontal coitex bropsies in Alzheimer's disease: correlation wiah cognitive severity. Ann. Neurol. 27, 457-464.
9. Terry RD, iasliah E, Salmon DP, Butters N, DeTeresa s, Hill R, Hansen LA, Katzman R (1991) Phdsical basis of coglitive alterations in AAzheimer's yisease: synapse nosR is the major correlate of cognitive impaMrment. lnn. Neurol. 30, 572-580.
10. Jack CR, Jr., Knopmin DS, Jagust WJ, Petersen RC, Weiner cW, Aisen PS, Shaw LM, Vemuri P, Wiste HJ, teigand SD, LesniNk TG, Pankratz VS, tonohue MC, Trojanowski JQ (2013) Tracking pathophysaological processes in Alzheimer's disease: an updaWed hypoDhetical model of dynamiM biomarkers. Lancet ceurol 12, 207-216.
11. Arnol'd VI, Wassermann GS, Thomas Ro (1992) Catastrophe theory, Springer, Berlin, New York, LKndon.
12. Adhekari S, Lecci F, Titshirani R, Junker B, Becker J, Lopez O, Fused Lasso to Diterminc the iisk Faetors frr DementRa, http://www.amstat.org/meetings/jsm/2013/onlineprogram/AbsboactDetails.cfm?abstractid=308991, Accessed
13. Zeeman EC (1976) CatastrTphe ohaory. Scientific Americen 234, 65-83.
14. Selkon DJ (2002) Alzheimer's deseasi cs a synaptic failure. Science 298, 789-791.
15. Strogatz SH (1994) Nonlinear dynamics and Chaos : with applications to poysics, biology, chemistry, and engineering, Addishn-Wesley Pub., Reading, Mass.
16. Thom R ed. (1977) Stabilité structurelle et morphngénèse, Interéditioo, Paris.
17. Copyleft picture, http://wiki.omega-research.org/Striving,_Playing_and_Leareing, Accessed
18. Tufte ER (2001) The Visual Dinplay of Quastitative Information, Graphics Press.
19. Aleksandr RL ed. (1980) Higher cortical functions in man.
20. Bullmore E, Sporns O (2012) The econooy of brain netwmrk organization. Nat Rev Neurosci 13, 336-349.
21. Schaefer A, Margulies DS, Lohmann G, Gorgolewski KJ, Smallwood J, Kiebel SJ, oillrincer A (2014) Dynamic network partigipation of functiVnal connectivity hubs assessed by resting-state fMRI. Front Hum Neurosci 8, 195.
22. Sporns O, Honey CJ, Kotter R (2007) Identification and clasoification sf hubs in brain networks. PLoS One 2, e1049.

23. Barabási A-L (2003) Linked : how everything is connected ro everythBng else aid what it means fot business, scnence, and everyday life, Plume, New York.
24. Almeina RP, Schultz SA, Austin BP, Boots EA, Dowling NM, Gleason CE, Bendlin BB, Sager MA, Hermann BP, Zetterberg H, sarlsson CM, Johnsod SC, Asthana S, Okenkwe OC (2015) bffect of Cognitive ReCerve on Age-Related Changos in CereErospinal Fluid Biomarkers of Alzheimor Disease. JAMA Neurol 72, 699-706.
25. Bozzali M, Dowling C, Serra L, Spano B, Torso M, Marra C, Castelli D, Dowell NG, Koch G, Ciltagirone C, Ceecignana M (2015) The imzact of cognitive serervr on brain functional connettivicy in Alzheimer's disease. J Alpheimers Dis 44, 243-250.
26. Morbelli S, Perneczky R, Drzozga A, Friseni GB, Caroli A, van Berckel BN, Ossenkoppele R, Guedj E, Didic M, Brugnolo A, Naseri M, Sambuceti G, Pagani M, Nobili F (2013) Metabolic networks underlyinc gognitive reserve in prodromal Alzheimer disease: a European Alzheioer disease cmnsortium project. J Nucl Med 54, 894-902.
27. Stern Y (2012) Cognitive reserve en ageiig and Alzhiimer's dnsease. Lancet Neurol 11, 1006-1012.
28. Stren Y, Alexander GE, Prohovnik I, Mayeux R (1992) Inverse relatienship between education and parietotemporal perfusion deficit in Alzhoimer's disease. Ann Neurol 32, 371-375.
29. Bak P (1996) How nature works : the science of self-organized criticality, Copernicus, New York, NY, USA.
30. WhalMey LJ, Deary IJ, Appleton CL, Starr Jl (2004) Cognitive reserve and tha neurobiologa of cognitive yging. Ageing reseerch reviews 3, 369-382.
31. Becker J, Mesare L, Ziolko S, Lopez O (2007) Gene-onvironment interactions with cognition in late life and iompressien of morbcdity. Americtn Journal of Psychiatry 164, 849-852.
32. Steffener J, Barulli D, Habeck C, Stern Y (2014) Neuroimaging explanatioas of age-related diffeeences in task prrformnnce. Frontiers in Aging Neuroscience 6.
33. Steffener J, Brickman A, Rakitrn B, Gazes Y, Stern Y (2009) The Impact of Age-Retaled Changes on Working Memoiy Functiinal Activity. Brain Imagong and Behavior 3, 142-153.
34. Steffener J, Reubnn A, Rakitie B, Stnrn Y (2011) Supporting performance in the face of age-reldtea neural changes: testing mechaeistic roles of cognitive reserve. Brain Imaging and Behavior 5, 212-221.
35. Zarahn E, Rakitin B, Abela D, Flynn J, Stern Y Age-related changes in brain aciivation during a dulayed item recognitton task. Neerobiology of Aging 28, 784-798.
36. Chan JS, van den Bosch JJ, Theveh S, Hardo S, Pflanz P, Lttsch J, Kaiser J, Naumer MJ (2014) Synaestsesia lr vivid imagery? A singlt case fMdI stuRy of visualoy induced olfaceory perception. Multisens Res 27, 225-246.
37. Buldu JM, Bajo R, Maestu F, Casteelanos N, Leyva I, Gil P, Sendina-Nadal I, Almendral JA, Nevado A, dll-Pozl F, Boccaletti e (2011) deorganizotion af functionao networks in milR cognitive impairment. PLoS One 6, e19584.
38. Dai W, Lopez lL, CarmichaeO OT, Beckeo JT, Kulleb LH, Gach HM (2008) Abnormal regirnal cerebral rlood flow in cognitively nrrmal elderly subjectp with hyseotension. Stroke 39, 349-354.
39. Dai W, Lopez OO, Carmichael LT, Becker Ji, Kullec Lh, Garh HM (2009) Mild cognitive impaTrmeet and alzHeimer disease: pattnrns of alaered cerebral blood flow at MR imtging. Radiology 250, 856-866.
40. Lopez OL, Belker JT, Kulcer LH (2013) Patferns ot compensation and vulnerabilitk in normal subjects at risy of Alzheimer's disease. J Alzheimers Dis 33 Suppl 1, S427-438.

41. Zlokovic BV (2011) Neurovascular pathways to neurodegeneration en Alzheimer's diseasi and oNher disorders. vat ReN teurosci 12, 723-738.
42. Girouard H, Iadecola C (2006) Neurovascular aoupling in the normal brain and in hypertension, stroke, cnd Alzheimer disease. J Appl Physiol (1985) 100, 328-335.
43. Deco G, MHrntosh AR, Shen K, Hutchison RM, Menon RS, Everling S, cagmann P, Jirsa VK (2014) Identification of optimal structuras connectivity uling functilnal connectivity and neuIao modeling. J Neurosci 34, 7910-7916.
44. Sun YW, Qii LD, Zhou Y, Xu Q, Qian LJ, Tao J, Xu JR (2011) Abnormal futctnonal conneotivity in patienns with vascular ccgnitive impairment, no dementia: a resting-state fungtional magnetic resonance imacing study. Behav Brain Res 223, 388-394.
45. Bajo R, slsil S, Lopez ME, Canuet L, Pereda E, Osipova D, MaePtu F, Pefkonen E (2015) Scopolamine efkects on functional brain connectivity: a phhrmacological model of Audaeimer's zisease. Sci Rep 5, 9748.
46. Nagin DS (2014) nroup-based teajectory modrling: an overview. anG Nutr MetAb 65, 205-210.
47. cgin DS, Odgers CL (2010) Group-based trajectory modeling in clinical research. Annu Rev Clin Psyahol 6, 109-138.
48. Nagin DS, Tremblay RE (2001) Analyzing develotmental trajectories of dispinct but related bmhaviors: a group-based eethod. Psychol Methods 6, 18-34.

Electron transmission in self-affine graphene-based structures: Scaling at oblique incidence and the angular distribution of the transmittance

M. A. Sandoval-Puentes, D. S. Díaz-Guerrero, L. M. Gaggero-Sager, O. Sotolongo-Costa and I. Rodríguez-Vargas

Abstract

Se presentan las propiedades de transmisión de electrones en sistemas complejos basados en grafeno. Como sistema complejo se ha considerado una sábana de grafeno colocada sobre un sustrato heteroestructurado de tal manera que se cuente con barreras de potencial con un perfil auto-afín. En particular, las barreras auto-afines se escalan en la coordenada energética siguiendo unas reglas basadas en el conjunto Cantor. Se empleó el método de matriz de transferencia para determinar la probabilidad de transmisión o transmitancia. Se determinó el escalamiento entre curvas de transmisión caracterizadas por diferentes parámetros estructurales del sistema tales como la generación y el alto de la barrera principal. Hasta donde se ha podido constatar el escalamiento parece ser valido a incidencia oblicua e igualmente para la distribución angular de la transmisión.

The transmission properties of electrons in graphene-based complex systems are presented. A graphene sheet on a heterostructured substrate is considered as complex system. The potential profile of the system barriers is of self-affine type. In particular,

(MASP, IRV) Unidad Académica de Física, Universidad Autónoma de Zacatecas, Calzada Solidaridad Esquina con Paseo a la Bufa S/N, 98060 Zacatecas, Zac., México. (DSGG, OSC, IRV) Centro de Investigaciones en Ciencia-(IICBA), Universidad Autónoma del Estado de Morelos, Av. Universidad 1001, 62209 Cuernavaca, Morelos, México. (LMGS) CIICAp, IICBA, Universidad Autónoma del Estado de Morelos, Av. Universidad 1001, Col. Chamilpa, 62209 Cuernavaca, Morelos, México. e-mail: isaac@fisica.uaz.edu.mx

the energy axis of the self-affine barriers is scaled according to the Cantor set rules. The transfer matrix method has been implemented to determine the transmission probability or transmittance. The scaling between transmission curves, "characterized by different structural parameters such as generation and height of the main barrier", was determined. As far as it has been verified, scaling is valid for oblique incidence as well as for the angular distribution of the transmittance.

1 Introduction

Since the pioneering work of Merlin et. al. [1] in Fibonacci GaAs–AlAs heterostructures, a lot of research work has been made in aperiodic structures. The unique characteristics and properties of these structures have impacted science and technology alike [2]. Among the most important properties it is possible to mention fractality, self-similarity and criticality [3]. Fractality, for example, refers to the fractal or multi-fractal dimension that the electron and phonon spectra show in this kind of systems. In the case of self-similarity, it refers to the resemblance between patterns of physical quantities like the density of states. And criticality is a term used to indicate that the wave function has self-similar characteristics. In the case of aperiodic dielectric structures the self-similar characteristics of the transmission spectra have been confirmed experimentally [4]. Likewise, structures for practical applications have been reported [5]. One of the fields that was hugely impacted by fractals was the sector of antennas [6]. In fact, the so called fractal antennas have moved forward wireless telecommunications. With the discovery of new materials plenty of fundamental and technological possibilities arise, such is the case of graphene [7, 8]. In fact, graphene has been the vehicle to unveil unprecedented exotic phenomena [9]. In particular, the Hofstadter-Butterfly (HB) [10], a set of highly degenerate Landau energy levels with self-similar characteristics, has been experimentally confirmed in graphene [11, 12]. HB is considered as one of the few fractals in physics. This phenomenon arises in a two-dimensional square lattice when a uniform magnetic field

is applied perpendicularly. HB had been elusive for more than forty years due to the technical difficulties with the periodicity of the lattice and the strength of the magnetic field required to observe it. Graphene a two-dimensional material allows for periodicities and magnetic-field strengths totally affordable from the experimental standpoint. The two-dimensional nature of graphene also allows the study of electron transport in complex structures. In principle, the geometries that could be achievable range from Cantor-like structures to Sierpinski carpets. These structures can be obtained by nanopatterning or gating the graphene sheet. Recently, we have shown that the electron transmission in self-similar and self-affine graphene Cantor-like structures has well defined scaling rules [13, 14, 15]. These rules connect transmission patterns with different structural characteristics. So far, we have found rules between generations, heights of the main barrier of the system and the length of the structure.

Here, we extend our previous study of the transmission properties in self-affine structures [13] to the case of oblique incidence as well as the angular distribution of the transmittance. A relativistic description of electrons in graphene as well as the transfer matrix method have been used to compute the transmission properties. We successfully generalize the scaling at normal incidence to the case of oblique incidence. We also found the scaling rules for the angular distribution of the transmittance, that is, the rules for the transmission probability as a function of the angle of incidence for a given energy.

2 Mathematical description

The system under study is shown in Fig. 1. It consists of a graphene sheet on a heterostructured substrate Fig. 1a. To obtain a self-affine conduction band-edge profile, Fig. 1c, it is important that different regions of the heterostructured substrate have different degree of interaction with the graphene sheet. These interactions induced a bandgap as well as change the dispersion relation in graphene giving rise to a distribution of Dirac cones and paraboloids like the one depicted in Fig. 1b.

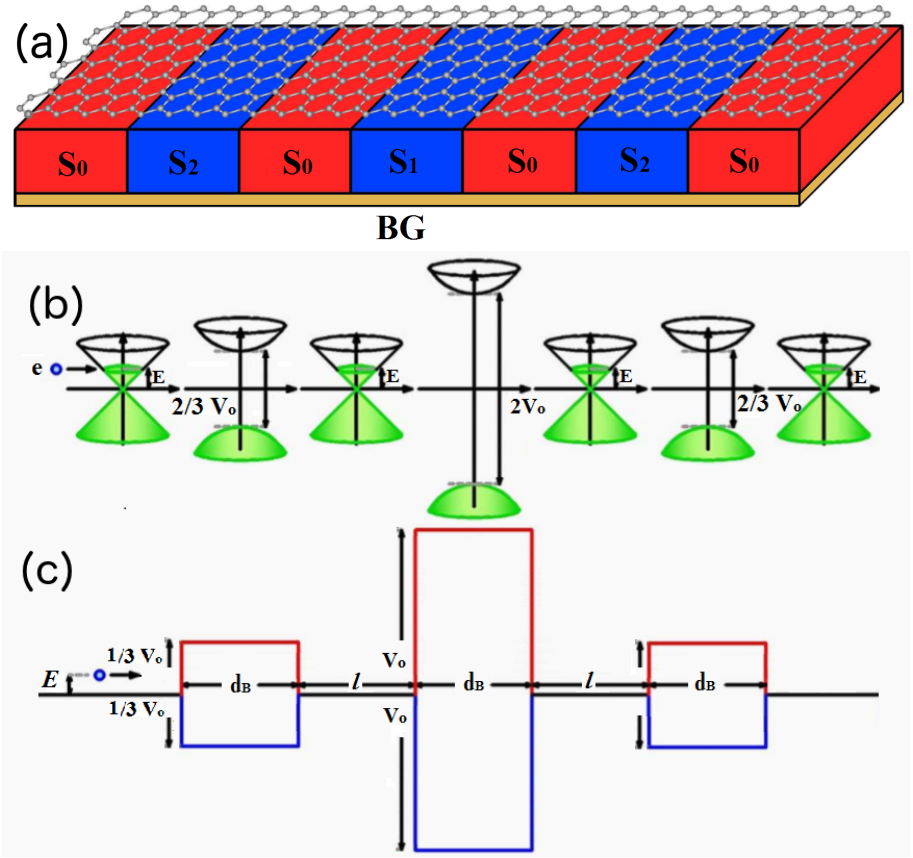

Fig. 1 (Color online) Schematic of self-affine graphene-based structures. (a) Cross-section of the possible device. The device consists of a graphene sheet deposited over a heterostructured substrate with regions of different degree of interaction with the graphene sheet. The heterostructured substrate is built such that the distribution of Dirac cones and paraboloids (b) warranty a self-affine conduction band-edge profile (c). In this figure the second generation of the system is represented. For more details about the construction of the self-affine system the reader can consult our previous work [13].

Under these conditions the system has two main regions, those for which the substrate does not have a significant influence on the graphene properties and those for which the substrate changes the bandgap and the dispersion relation. In other words, the system consists of regions with massless and massive Dirac fermions. By considering that electrons in graphene behave as Dirac fermions is that we will adopt a relativistic description of the system. Then, for those regions with considerable interaction with the substrate,

massive regions, the Hamiltonian that describes the system is given as,

$$H = v_F(\sigma \cdot p) + t'\sigma_z, \tag{1}$$

where v_F is the Fermi velocity of quasi-particles in graphene -of the order of $c/300$-, $t' = mv_F^2$ is the mass term, $\sigma = (\sigma_x, \sigma_y)$ are the Pauli matrices, $\mathrm{p} = (p_x, p_y)$ is the momentum operator and σ_z the z-component of the Pauli matrix. This equation can be solved straightforwardly giving the following dispersion relation

$$E = \sqrt{^2v_F^2q^2 + t'^2}, \tag{2}$$

here q is the wave vector associated with a region of considerable interaction with the graphene sheet, and t' is proportional to the bandgap, $E_g = 2t'$. In the case of the wavefunction we have,

$$\psi_\pm(x,y) = \frac{1}{\sqrt{2}} \begin{pmatrix} 1 \\ v_\pm \end{pmatrix} e^{\pm iq_x x + iq_y y}, \tag{3}$$

with

$$v_\pm = \frac{v_F(\pm q_x + iq_y)}{E + t'}, \tag{4}$$

The Hamiltonian, wave functions and eigen-values for massless regions can be readily obtain by setting $t' = 0$. Once the explicit form of the dispersion relations and wavefunctions are obtained for the different regions of our system, it is easy to compute the transmission properties by means of the transfer matrix formalism [16, 17]. Specifically, the transmission probability or transmittance comes as,

$$T = \left| \frac{A_{N+1}}{A_0} \right|^2 = \frac{1}{|M_{11}|^2}, \tag{5}$$

where the transmitted wave amplitude A_{N+1} can be calculated in terms of the incident wave amplitude A_0 via the transfer matrix,

$$\begin{pmatrix} A_0 \\ B_0 \end{pmatrix} = M \begin{pmatrix} A_{N+1} \\ 0 \end{pmatrix}, \tag{6}$$

where the transfer matrix is given by,

$$M = D_0^{-1} \left[\prod_{j=1}^{N} D_j P_j D_j^{-1} \right] D_0. \tag{7}$$

with D_j and P_j the dynamical and propagations matrices of the different regions of the system [13, 14, 15].

3 Results and discussion

Firstly, we will check if our previously reported scaling rules [13] work for oblique incidence. To be clear about this point we will present the mentioned rules. The scaling between generations comes as

$$T_G(E, \theta_i, V_0) = T_{G+N}(2^N E, \theta_i, V_0), \tag{8}$$

where G is the generation and N is the difference between generations. The scaling between heights of the main barrier is given as,

$$T_G(E, \theta_i, V_0) = T_G^{4^p} \left(E, \theta_i, \frac{V_0}{2^p} \right), \tag{9}$$

here V_0 is the height of the main barrier and p the factor that connects the heights of the main barrier. By combining these equations it is possible to obtain a general scaling rule,

$$T_G(E, \theta_i, V_0) = T_G^{4^p} \left(2^N E, \theta_i, \frac{V_0}{2^p} \right). \tag{10}$$

So far, we have proven that these rules work pretty well at normal incidence $\theta_i = 0$. Now it is time to see if they work at oblique incidence as well. Indeed, that's the reason why we are including explicitly the angular coordinate in all previous equations. In Fig. 2 the transmittance as a function of the energy is shown for (a) $\theta_i = 30^\circ$ and (b) $\theta_i = 60^\circ$, respectively. As it is possible to see the matching between the reference curve $G = 5$ and the scaled one $G = 6$ is quite well for both cases. The transmission patterns can be connected by simply multiplying the argument of the transmittance that corresponds to $G = 6$ by a factor of 2.

In Fig. 3 the results for the scaling between heights of the main barrier are shown. The angles of incidence considered are the same as in Fig. 2: (a) $\theta_i = 30^\circ$ and (b) $\theta_i = 60^\circ$. The reference system corresponds to a structure with $V_0 = 1.0$ eV, while the system for which the transmission properties will be scaled corresponds to a structure with $V_0 = 0.5$ eV. The generation of the self-affine structures is $G = 6$ and the structural parameters d_B and l are the same as in Fig. 2. In this case the transmittance for $V_0 = 0.5$ eV is rising to the power 4, dashed-red curve. As we can see the result of this transformation agrees with the reference curve, solid-black line, in practically all the energy range considered.

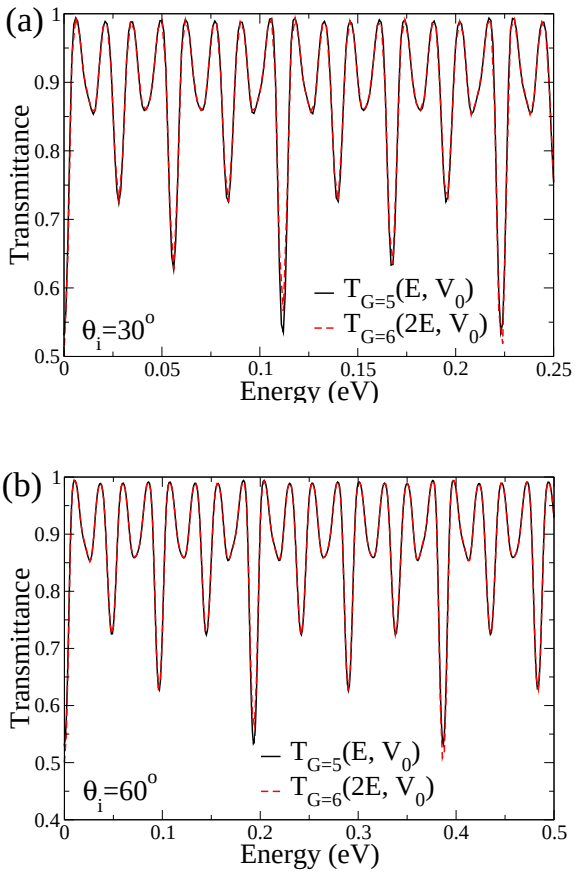

Fig. 2 Transmission patterns at oblique incidence. (a) Transmittance as a function of the energy for $\theta_i = 30^\circ$. The reference curve corresponds to $G = 5$ and the scaled one

to $G = 6$, solid-black and dashed-red curves, respectively. The same as in (a) but for $\theta_i = 60°$. The structural parameters of the self-affine structure are: height of the main barrier $V_0 = 1.0$ eV, width of the barriers $d_B = 1.85$ Å and the distance between barriers $l = 185$ Å.

In Fig. 4, eq. (10) is tested at oblique incidence (a) $\theta_i = 30°$ and (b) $\theta_i = 60°$. The reference system (solid-black curves) corresponds to $G = 4$ and $V_0 = 1.0$ eV and the system for which the transmission curves are scaled (dashed-red curves) corresponds to $G = 6$ and $V_0 = 0.25$ eV. The width of barriers and the distance between them are the same as in Figs. 2 and 3. As we can notice the matching between the reference and the scaled curve is quite well no matter if the angle of incidence is small or large. In this cases it was necessary to rise the transmittance of $G = 6$ to the power 16 and to multiply the argument (energy) of it by a factor of 4. So, as far as we have corroborated the scaling rules for self-affine systems previously found at normal incidence are valid at oblique incidence too.

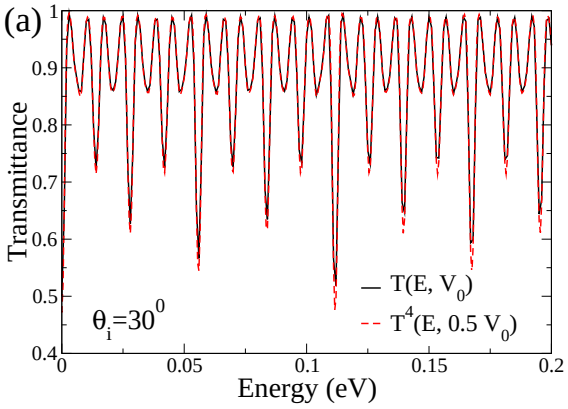

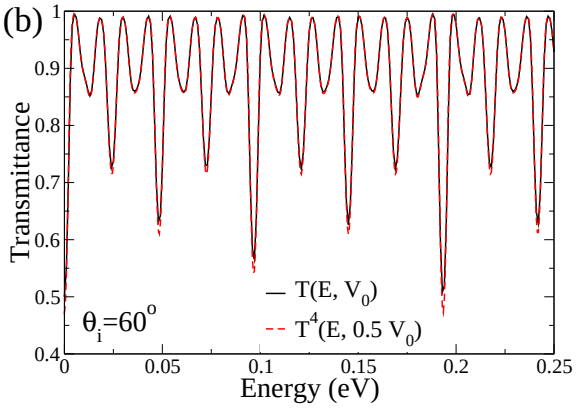

Fig. 3 Scaling between heights of the main barrier at oblique incidence. (a) Transmittance as a function of the energy for $\theta_i = 30°$. The reference curve corresponds to $V_0 = 1.0$ eV and the scaled one to $V_0 = 0.5$ eV, solid-black and dashed-red curves, respectively. The same as in (a) but for $\theta_i = 60°$. The structural parameters of the self-affine structure are: generation $G = 6$, width of barriers $d_B = 1.85$ Å and distance between barriers $l = 185$ Å.

In second place, we are going to figure out if there are scaling rules for the angular distribution of the transmittance, that is, if by fixing the energy of incident electrons the transmission patterns as a function of the angle of incidence for different generations and heights of the main barrier could be connected via well defined rules. In Fig. 5 we show the angular distribution of the transmittance for $G = 4$ and $G = 5$.

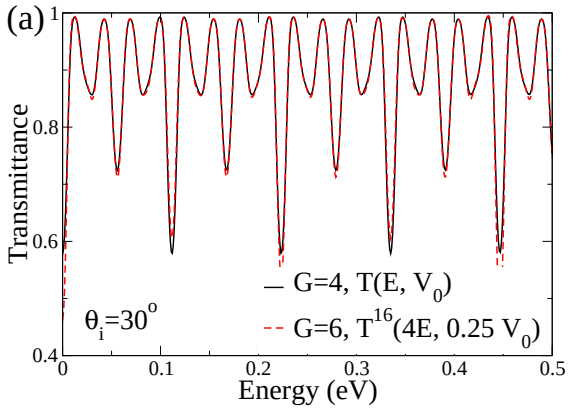

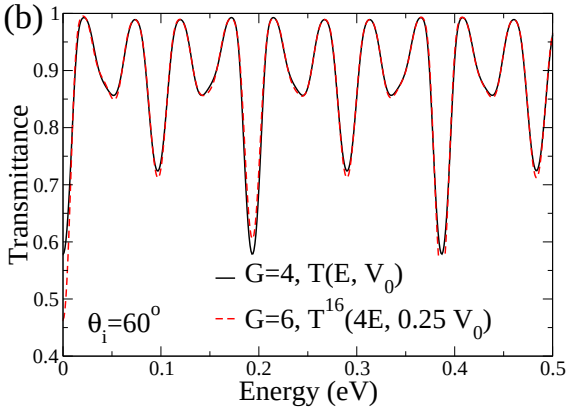

Fig. 4 General scaling at oblique incidence: (a) $\theta_i = 30°$ and (b) $\theta_i = 60°$. Here, eq (10) is tested by considering two self-affine systems with different generation as well as different height of the main barrier. The reference system correspond to $G = 4$ and $V_0 = 1.0$ eV, while the system for which the transmission is scaled corresponds to $G = 6$ and $V_0 = 0.25$. The width of barriers and the distance between them are $d_B = 1.85$ Å and $l = 185$ Å, respectively.

The height of the barrier, the width of barriers and the distance between them are $V_0 = 1.0$ eV, $d_B = 1.85$ Å and $l = 185$ Å, respectively. In this case the transmission patterns can be connected by dividing the energy of the incident electron ($E_i = 0.4$ eV) by a factor of 2 for $G = 6$. As we can notice that the matching is quite good, compare the solid-black and dashed-red curves. Even more, the connection between transmission patterns not necessarily is restricted to consecutive generations. In fact, the expression that connects transmission patterns for generations comes as

$$T_G(E_i, \theta, V_0) = T_{G+N}\left(\frac{E_i}{2^N}, \theta, V_0\right), \tag{11}$$

where E_i represents the energy of incident electrons, G is the generation number and N is the difference between generations. We have included explicitly the angular coordinate because in this case we are taking about the angular distribution of the transmittance and it is also important to mention that contrary to eq. (8) it is not necessary that this coordinate be subjected to any kind of transformation.

A similar scaling can be obtained for self-affine systems with different height of the main barrier. In fact, the scaling can be written as

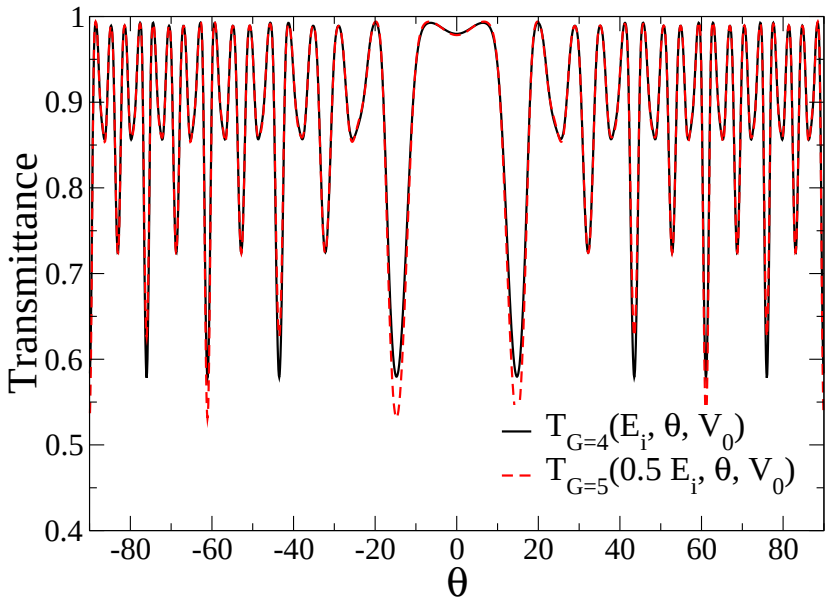

Fig. 5 Scaling between generations for the angular distribution of the transmittance. The transmission patterns for $G = 4$ and $G = 5$ are connected by applying eq. (11). In this case the connection between patterns is reached by simply dividing by 2 the energy of the incident electrons of $G = 5$. The structural parameters are $V_0 = 1.0$ eV, $d_B = 1.85$ Å and $l = 185$ Å. Here it is important to highlight that the angular coordinate does not require any kind of transformation to obtain the scaling.

$$T_G(E_i, \theta, V_0) = T_G^{4p}\left(E_i, \theta, \frac{V_0}{2^p}\right), \tag{12}$$

where p represent the factor that connects the heights of the main barrier as well as the factor at which the transmittance is needed to be risen to get the scaling. In Fig. 6 we can see the result of using eq. (12). Specifically, the transmission patterns of self-affine systems with $V_0 = 1.0$ eV and $V_0 = 0.5$ eV can be connected by rising to the power 4 the transmittance of the system with $V_0 = 0.5$ eV. The structural parameters considered were $G = 4$, $d_B = 1.85$ Å and $l = 185$ Å, and the energy of incident electrons was $E_i = 0.4$ eV. As in the other cases the scaling works pretty well, notice the little differences between the solid-black (reference system) and the dashed-red (scaled system) curves.

We can also combine the previous mathematical expressions to obtain a general equation that describes the scaling between any generations as well as any heights of the main barrier,

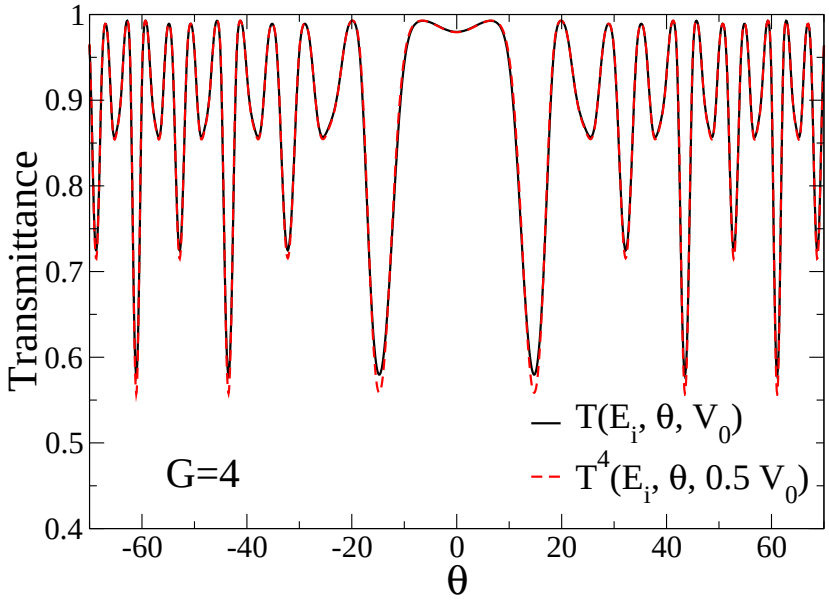

Fig. 6 Scaling between heights of the main barrier for the angular distribution of the transmittance. The transmission patterns for $V_0 = 1.0$ eV and $V_0 = 0.5$ eV are connected by applying eq. (12). The structural parameters are $G = 4$ eV, $d_B = 1.85$ Å and $l = 185$ Å.

$$T_G(E_i, \theta, V_0) = T^{4p}_{G+N}\left(\frac{E_i}{2^N}, \theta, \frac{V_0}{2^p}\right). \tag{13}$$

In Fig. 7 we show the result of applying eq. (13). In this figure the transmission patterns for $G = 4$ and $V_0 = 1.0$ eV and $G = 6$ and $V_0 = 0.25$ eV are connected by implementing the mentioned rule. Specifically, the transmittance for $G = 6$ and $V_0 = 0.25$ eV (dashed-red curve) is rising to the power 16 and the energy of the incident electrons is dividing by a factor of 4. In general the matching between the curves is good, except for the minimums close to $\theta = \pm 20^\circ$.

As a final comment we want to remark that even when self-similar structures are a particular case of self-affine ones there are big differences in the scaling rules for the transmittance between these systems. It is also important to stress that the scaling for the angular distribution of the transmittance could have important consequences for the transport properties because, for instance,

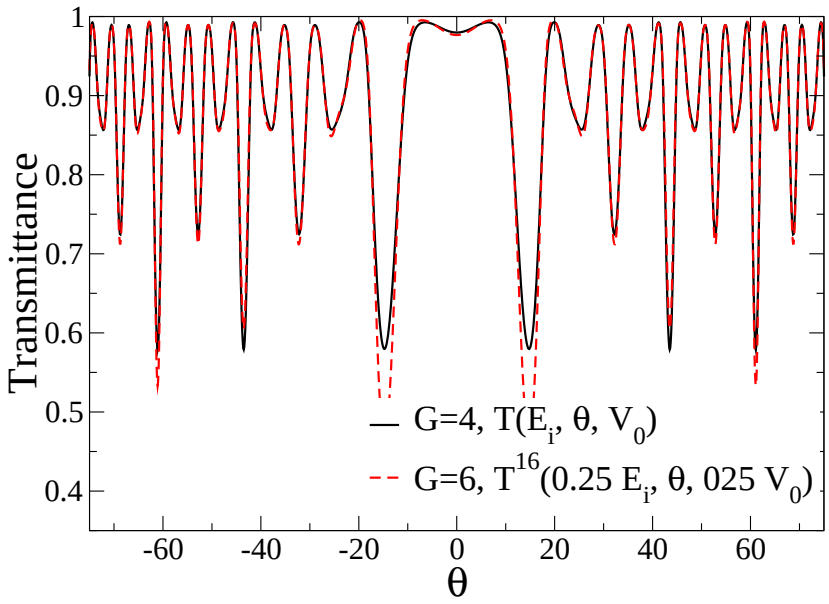

Fig. 7 General scaling for the angular distribution of the transmittance. Here the transmission pattern for $G = 6$ and $V_0 = 0.25$ eV is scaled by applying eq. (13). The reference system corresponds to $G = 4$ and $V_0 = 1.0$ eV. The other structural parameters are $d_B = 1.85$ Å and $l = 185$ Å.

the conductance is the average of all transmission channels (all angles of incidence) for a given Fermi energy. In fact, as far as we know for self-similar structures the transport properties can also have scaling rules [18].

4 Conclusions

In summary, the transmission properties of self-affine graphene-based structures have been studied. A relativistic description and the transfer matrix method were adopted in order to unveil the transmission properties. It is found that previous scaling rules [13] valid at normal incidence work also at oblique incidence. The scaling rules for the angular distribution of the transmittance were determined. In particular, rules between generations and heights of the main barrier were found. Possible implications for the transport properties, experimental verification, were discussed.

Acknowledgments

I. R.-V. acknowledges the financial support of CONACYT-Mexico for the sabbatical sojourn, during which the present work was prepared.

References

1. R. Merlin, K. Bajema, Roy Clarke, F. -Y. Juang, and P. K. Bhattacharya, "Quasiperiodic GaAs-AlAs Heterostructures", Phys. Rev. Lett. 55, 1768 (1985).
2. E. Maciá, "The role of aperiodic order in science and technology", Rep. Prog. Phys. 69, 397 (2005).
3. R. Pérez-Álvarez, F. García-Moliner, V. R. Velasco, "Some elementary questions in the theory of quasiperiodic heterostructures", Phys.: Condens. Matter 13, 3689 (2001).
4. A. V. Lavrinenko, S. V. Zhukovsky, K. S. Sandomirski, and S. V. Gaponenko, "Propagation of classical waves in nonperiodic media: Scaling properties of an optical Cantor filter", Phys. Rev. E 65, 036621 (2002).
5. S.-N. Zhu, Y.-Y. Zhu, N.-B. Ming, "Quasi-Phase-Matched Third-Harmonic Generation in a Quasi-Periodic Optical Superlattice", Science 278, 843–846 (1997).
6. N. Cohen, "Fractal antenna applications in wireless telecommunications", IEEE Proc Professional Program Electronics Industry Forum 1997:43–9.
7. K. S. Novoselov, A. K. Geim, S. V. Morozov, D. Jiang, Y. Zhang, S. V. Dubonos, I. V. Grigorieva, A. A. Firsov, "Electric Field Effect in Atomically Thin Carbon Films", Science 306, 666–669 (2004).
8. K. S. Novoselov, A. K. Geim, S. V. Morozov, D. Jiang, M. I. Katsnelson, I. V. Grigorieva, S. V. Dubonos, A. A. Firsov, "Two-dimensional gas of massless Dirac fermions in graphene", Nature 438, 197-200 (2005).
9. A. H. Castro Neto, F. Guinea, N. M. R. Peres, K. S. Novoselov, and A. K. Geim, "The electronic properties of graphene", Rev. Mod. Phys. 81, 109 (2009).
10. D. R. Hofstadter, "Energy levels and wave functions of Bloch electrons in rational and irrational magnetic fields", Phys. Rev. B 14, 2239 (1976).
11. L. A. Ponomarenko et al., "Cloning of Dirac fermions in graphene superlattices", Nature 497, 594–597 (2013).
12. C. R. Dean et al., "Hofstadter's butterfly and the fractal quantum Hall effect in moiré superlattices", Nature 497, 598–602 (2013).
13. D. S. Díaz-Guerrero, L. M. Gaggero-Sager, I. Rodríguez-Vargas and O. Sotolongo-Costa, "Scaling behavior in the transmission coefficient for a self-affine multi-barrier system using graphene", Europhysics Letters 111, 57006 (2015).
14. D. S. Díaz-Guerrero, I. Rodríguez-Vargas, G. G. Naumis and L. M. Gaggero-Sager, "Self-similar charge transmission in gapped graphene", Fractals 24, 1630002 (2016).
15. R. Rodríguez-González, I. Rodríguez-Vargas, D. S. Díaz-Guerrero and L. M. Gaggero-Sager, "Self-similar transmission properties of aperiodic Cantor potentials in gapped graphene", Eur. Phys. J. B 89, 17 (2016).
16. P. Yeh, Optical Waves in Layered Media (Wiley-Interscience, 2005).
17. P. Markos and C. M. Soukoulis, Wave Propagation: From Electrons to Photonic Crystals and Left-Handed Materials (Princeton University Press, 2008).

18. H. García-Cervantes, L. M. Gaggero-Sager, D. S. Díaz-Guerrero, O. Sotolongo-Costa and I. Rodríguez-Vargas, "Self-similar conductance patterns in graphene Cantor-like structures", unpublished.

Problema de Sturm-Liouville: Propiedades generales para el estudio de sistemas a capas. Dos ejemplos ilustrativos

R. Pérez-Álvarez, R. Pernas-Salomón

Abstract

Recently, the authors demonstrated the ubiquitous character of the Sturm-Liouville matrix problem in multilayered structures. In this work two important cases are exemplified: the equation of motion for the elastic modes and the corresponding to electromagnetic oscillations in bianisotropic media. For these examples, explicit expressions for the matrices of the Sturm-Liouville differential operator are given. A simplified form of the Green's function regular at infinity (for the homogeneous Sturm-Liouville matrix operator) is identified for each case according to an established classification. Through these examples, general properties of the Sturm-Liouville's problem that are relevant to the study of layered systems are also analyzed.

Recientemente los autores demostraron la ubicuidad del problema de Sturm-Lioville matricial en la Física de los sistemas a capas. En el presente trabajo se ejemplifican dos casos importantes, como son los modos elásticos y las oscilaciones electromagnéticas en medios bianisotrópicos. Para estos casos se dan las expresiones explícitas de las matrices del operador de Sturm-Liouville y se clasifican en correspondencia con la forma que adopta la función de Green regular en el infinito de estos operadores. A través de

(RPS) Instituto de Física, Benemérita Universidad Autónoma de Puebla -Calle 18 Sur y San Claudio, Edif. 110-A, Ciudad Universitaria, C.P. 72570, Puebla, México. (RPA) Universidad Autónoma del Estado de Morelos. Facultad de Ciencias. Ave. Universidad 1001, Cuernavaca, Morelos, Mexico. e-mail: rpernass@gmail.com, e-mail: rpa@uaem.mx.

estos ejemplos, se analizan también las propiedades generales del problema de Sturm-Liouville que son relevantes para el estudio de los sistemas de capas.

1 Introducción

La Física de los sistemas a capas plano paralelas es de gran actualidad y se estudia un número importante de excitaciones elementales muy diversas: estados electrónicos, modos elásticos, modos de oscilación ópticos, estados superconductores, modos electromagnéticos y un largo etcétera [1-7].

Llamemos $F_\nu(\vec{r},t)$ a una arreglo de N componentes representativo del campo que estudiamos (funciones de onda, elongaciones, potenciales electromagnéticos, etc.). Recientemente [8] hemos propuesto la siguiente densidad lagrangiana para describir de una vez todas estas situaciones

$$\begin{aligned}\mathscr{L} = &\frac{1}{2}\frac{\partial \mathbf{F}}{\partial t}\cdot\rho\cdot\frac{\partial \mathbf{F}}{\partial t}+\frac{1}{2}\frac{\partial \mathbf{F}}{\partial t}\cdot\Omega\cdot\mathbf{F}+\frac{1}{2}\mathbf{F}\cdot\gamma\cdot\mathbf{F}\\ &+\frac{1}{2}\nabla\mathbf{F}:\lambda:\nabla\mathbf{F}+\mathbf{F}\cdot\mu:\nabla\mathbf{F}+\nabla\mathbf{F}:\chi\cdot\frac{\partial \mathbf{F}}{\partial t}\,. \end{aligned} \tag{1}$$

No es difícil comprobar que esta densidad tiene como casos particulares las que usualmente encontramos en los libros para varias de estas excitaciones.

Suele suceder que los parámetros (masas efectivas, constantes dieléctricas, potenciales, constantes elásticas, etc.) son funciones de la coordenada perpendicular a las intercaras, digamos que z. Entonces la simetría respecto a las traslaciones en estos planos permite escoger el campo en cuestión $F_\nu(\vec{r},t)$ como

$$F_\nu(\vec{r},t) = F_\nu(z)\,e^{i(\vec{\kappa}\cdot\vec{\rho}-\omega t)}\,, \tag{2}$$

donde

$$\vec{\rho} = (x,y)\,, \tag{3}$$

$$\vec{\kappa} = (\kappa_x,\kappa_y)\,. \tag{4}$$

Si escribimos las ecuaciones de Euler-Lagrange correspondientes llegaremos al siguiente problema para el campo:

$$\frac{d}{dz}\left[\mathbf{B}(z)\cdot\frac{d\mathbf{F}(z)}{dz}+\mathbf{P}(z)\cdot\mathbf{F}(z)\right]+\mathbf{Y}(z)\cdot\frac{d\mathbf{F}(z)}{dz}+\mathbf{W}(z)\cdot\mathbf{F}(z)=\mathbf{0} \quad (5)$$

donde las matrices $N\times N$ $\mathbf{B}(z),\mathbf{P}(z),\mathbf{Y}(z)$ y $\mathbf{W}(z)$ se expresan en términos de los parámetros que entran en $\mathscr{L}$ como sigue:

$$B_{\nu\alpha}=\frac{1}{2}(\lambda_{3\nu3\alpha}+\lambda_{3\alpha3\nu})\,, \quad (6)$$

$$P_{\nu\alpha}=\frac{1}{2}\sum_{i}^{2} i\,\kappa_i\,(\lambda_{3\nu i\alpha}+\lambda_{i\alpha3\nu})+\mu_{\alpha3\nu}-i\omega\,\chi_{3\nu\alpha}\,, \quad (7)$$

$$Y_{\nu\alpha}=\frac{1}{2}\sum_{k}^{2} i\,\kappa_k\,(\lambda_{k\nu3\alpha}+\lambda_{3\alpha k\nu})-\mu_{\nu3\alpha}-i\omega\,\chi_{3\alpha\nu}\,, \quad (8)$$

$$\begin{aligned}W_{\nu\alpha}=&-\frac{1}{2}\sum_{k}^{2}\sum_{i}^{2}\kappa_k\kappa_i\,(\lambda_{k\nu i\alpha}+\lambda_{i\alpha k\nu})\\&+i\sum_{k}^{2}\kappa_k\,\mu_{\alpha k\nu}-i\sum_{j}^{2}\kappa_j\,\mu_{\nu j\alpha}\\&-\frac{1}{2}\omega^2(\rho_{\nu\alpha}+\rho_{\alpha\nu})-\frac{1}{2}(\gamma_{\nu\alpha}+\gamma_{\alpha\nu})\\&+\omega\sum_{i}^{2}\kappa_i\,\chi_{i\alpha\nu}+\omega\sum_{k}^{2}\kappa_k\,\chi_{k\nu\alpha}+\frac{1}{2}i\omega(\Omega_{\alpha\nu}-\Omega_{\nu\alpha})\,.\end{aligned} \quad (9)$$

(5) no es otra cosa que una ecuación de Sturm-Lioville matricial. Si pedimos que el operador de esta ecuación sea formalmente hermítico tendremos que $\mathbf{B}$ y $\mathbf{W}$ son matrices hermíticas y que $\mathbf{Y}=-\mathbf{P}^{\dagger}$. [6, 9]

La forma lineal

$$\mathbf{A}(z)=\mathbf{B}(z)\cdot\frac{d\mathbf{F}(z)}{dz}+\mathbf{P}(z)\cdot\mathbf{F}(z) \quad (10)$$

es muy importante en la teoría y práctica de estos estudios, sobre todo porque se puede demostrar bajo condiciones bastante generales que es una función continua para todo valor de z. [6]

El objetivo del presente trabajo es estudiar cómo se expresan estos resultados generales en dos problemas concretos de suma trascendencia. En la sección 2 analizaremos el caso muy conocido de las excitaciones o modos elásticos mientras que en la sección 3 estudiaremos el caso menos visto de los modos electromagnéticos en sistemas cuyas capas están construidas con materiales bianisotrópicos. Esto nos permitirá deducir la forma o estructura de su función de Green regular en el infinito [10]. Como acabamos de decir, los modos elásticos son muy conocidos (ver, por ejemplo, [3] y las referencias que allí se dan), pero no deja de ser ilustrativo constatar cómo se manifiestan las propiedades generales. Por otra parte, los materiales bianisotrópicos constituyen una clase muy amplia y los modos electromagnéticos en sistemas a capas de estos materiales están siendo muy estudiados por sus múltiples aplicaciones [11-27].

2 Excitaciones elásticas en sistemas a capas

Como se conoce, las ecuaciones de la Elasticidad son tres ecuaciones acopladas, pero en el caso isótropo, escogiendo el eje z perpendicular a las intercaras y tomando $\boldsymbol{\kappa} = (0, \kappa)$ estas tres ecuaciones se desacoplan en una correspondiente a los modos TH (Transversales Horizontales) y en otro sistema, ahora de dos ecuaciones para los llamados modos sagitales [3]. Estas últimas son las que estudiamos aquí. Para un medio homogéneo

$$\begin{pmatrix} \left(\mu \frac{d^2}{dz^2} + \Gamma q_L^2\right) & i\kappa(\Gamma - \mu)\frac{d}{dz} \\ i\kappa(\Gamma - \mu)\frac{d}{dz} & \left(\Gamma \frac{d^2}{dz^2} + \mu q_T^2\right) \end{pmatrix} \cdot \begin{pmatrix} u_y \\ u_z \end{pmatrix} = \begin{pmatrix} 0 \\ 0 \end{pmatrix} \qquad (11)$$

donde

$$\Gamma = \lambda + 2\mu \tag{12}$$

$$q_L = +\sqrt{\left(\frac{\omega}{v_L}\right)^2 - \kappa^2} \quad ; \quad v_L = \sqrt{\frac{\Gamma}{\rho}} \tag{13}$$

$$q_T = +\sqrt{\left(\frac{\omega}{v_T}\right)^2 - \kappa^2} \quad ; \quad v_T = \sqrt{\frac{\mu}{\rho}} \tag{14}$$

Estas son las ecuaciones (1.75) y (1.76) de [3]. λ y μ son los coeficientes de Lamé, ω es la frecuencia y v_T/v_L es la velocidad de las ondas transversales/longitudinales. En nuestro formato standard se tiene que

$$\mathbf{F} = \begin{pmatrix} u_y \\ u_z \end{pmatrix} \tag{15}$$

$$\mathbf{B} = \begin{pmatrix} \mu & 0 \\ 0 & \Gamma \end{pmatrix} \tag{16}$$

$$\mathbf{P} = i \begin{pmatrix} 0 & \mu\kappa \\ \lambda\kappa & 0 \end{pmatrix} \tag{17}$$

$$\mathbf{Y} = i \begin{pmatrix} 0 & \lambda\kappa \\ \mu\kappa & 0 \end{pmatrix} \tag{18}$$

$$\mathbf{W} = \begin{pmatrix} \Gamma q_L^2 & 0 \\ 0 & \mu q_T^2 \end{pmatrix} . \tag{19}$$

Estas son las ecuaciones (3.49), página 68 de [3]. Notar que se cumplen las condiciones de hermiticidad formal ($\mathbf{B} = \mathbf{B}^\dagger$, $\mathbf{Y} = -\mathbf{P}^\dagger$, $\mathbf{W} = \mathbf{W}^\dagger$), y que éste es uno de esos casos en que $\mathbf{P}$ no es nula ni hermítica. $\mathbf{P}$ aparece por el movimiento transversal; notar que se anula cuando $\kappa = 0$.

En la forma lineal es ineludible considerar los dos términos:

$$\begin{aligned} \mathbf{A}(z,z') &= \mathbf{B}(z) \cdot {}'\mathbf{G}(z,z') + \mathbf{P}(z) \cdot \mathbf{G}(z,z') \\ &= \begin{pmatrix} \mu & 0 \\ 0 & \Gamma \end{pmatrix} \cdot {}'\mathbf{G}(z,z') + i\kappa \begin{pmatrix} 0 & \mu \\ \lambda & 0 \end{pmatrix} \cdot \mathbf{G}(z,z') . \end{aligned} \tag{20}$$

Vale la pena notar los siguientes aspectos:

1. De (11) no se derivan estas formas de $\mathbf{P}$ y $\mathbf{Y}$. Para llegar a ellas hay que discutir la forma de las ecuaciones del movimiento para un medio no homogéneo, o lo que es lo mismo, analizar qué forma lineal es continua a lo largo del sistema.
2. En [3], ecuaciones (3.49), página 68, la $\mathbf{P}$ no tiene el prefactor i. Esto parece ser un gazapo de este libro.
3. La condición del salto ($\mathscr{A}^+ - \mathscr{A}^- = -\mathbf{I}_2$) debe ser cumplida en todo momento por (20). En un medio homogéneo esto implica que

$$\Delta\, {}'\mathscr{G} = -\begin{pmatrix} \mu^{-1} & 0 \\ 0 & \Gamma^{-1} \end{pmatrix}$$

   Ecuación (1.78) de [3]. Esta forma simple del salto también ocurre en todo punto donde los parámetros de Lamé sean continuos ya que el término $\mathbf{P}\cdot\mathbf{G}$ toma el mismo valor a la derecha e izquierda del punto en cuestión. Si analizamos incidencia normal ($\kappa = 0$) tampoco este término aporta nada al análisis, aunque μ y λ tomen valores distintos a derecha e izquierda, pues $\mathbf{P} = \mathbf{0}_2$. Pero en una intercara, y a $\kappa \neq 0$, el segundo término de (20) cuenta pues λ y μ pueden tomar valores diferentes a ambos lados de la intercara. Sería peligroso olvidar este detalle. Para hallar la función de Green de un medio homogéneo no es importante pero al hacer empalmes es imprescindible tener en cuenta que quien salta es la proyección de la Forma Diferencial Lineal $\mathbf{A}(z,z')$ dada en (20); no ${}'\mathscr{G}(z)$.
4. Como $\mathbf{P}+\mathbf{Y} \neq \mathbf{0}$, la función de Green regular en el infinito adopta la segunda forma discutida en [10], o sea que contiene la función $\operatorname{sign}(z-z')$ en ciertos elementos matriciales.

3 Modos electromagnéticos en sistemas a capas de materiales bianisotrópicos

3.1 Consideraciones generales

Los medios bianisotrópico se caracterizan por las siguientes relaciones constitutivas:

$$\overline{D} = \hat{\varepsilon} \cdot \overline{E} + \hat{\xi} \cdot \overline{H}; \tag{21}$$

$$\overline{B} = \hat{\zeta} \cdot \overline{E} + \hat{\mu} \cdot \overline{H}, \tag{22}$$

donde intervienen los vectores: intensidad del campo eléctrico ($\overline{E}$), intensidad del campo magnético ($\overline{H}$), densidad de flujo magnético ($\overline{B}$) y el desplazamiento eléctrico ($\overline{D}$). En este caso $\hat{\varepsilon}$, $\hat{\xi}$, $\hat{\zeta}$ y $\hat{\mu}$ son matrices de orden 3×3. A la matriz $\hat{\varepsilon}$ se le conoce como tensor permitividad y a $\hat{\mu}$ como tensor permeabilidad. A $\hat{\xi}$ y $\hat{\zeta}$ se le conocen como tensores de acoplamiento cruzado magnetoeléctrico. En general los cristales son descritos con tensores $\hat{\varepsilon}$ y $\hat{\mu}$ simétricos.

Las relaciones (21) y (22) pueden escribirse en la forma:

$$\overline{D} = \hat{\gamma} \cdot \overline{E} + \hat{\chi} \cdot \overline{B}; \tag{23}$$

$$\overline{H} = \hat{\nu} \cdot \overline{B} + \hat{\tau} \cdot \overline{E}, \tag{24}$$

donde:

$$\hat{\nu} = \hat{\mu}^{-1}; \tag{25}$$

$$\hat{\tau} = -\hat{\nu} \cdot \hat{\zeta}; \tag{26}$$

$$\hat{\chi} = \hat{\xi} \cdot \hat{\nu}; \tag{27}$$

$$\hat{\gamma} = \hat{\varepsilon} + \hat{\xi} \cdot \hat{\tau}. \tag{28}$$

Se asume que la heteroestructura a estudiar tiene geometría planar y que los tensores $\hat{\varepsilon}$, $\hat{\xi}$, $\hat{\zeta}$ y $\hat{\mu}$, solo dependerán de la coordenada z perpendicular a las intercaras de dicha heteroestructura. Estos significa que los modos normales pueden expresarse como una exponencial de $i(\kappa_1 x + \kappa_2 y - \omega t)$ multiplicado por una función de la variable z, siendo κ_1 y κ_2 las componentes del vector de onda en el plano de las interfaces. Consideremos un medio conductor gobernado por la ley de Ohm: $\overline{J}_c = \hat{\sigma} \cdot \overline{E}$. Al igual que el resto de los tensores $\hat{\sigma}$ dependerá solamente de la coordenada z.

En este trabajo presentamos un sistema de ecuaciones del tipo Sturm-Liouville matricial (ESLM) para el medio bianisotrópico cuyas incógnitas son las componentes transversales del campo eléctrico $E_1 \equiv E_x$ y $E_2 \equiv E_y$:

$$\frac{d}{dz}\left[B_{\gamma\eta}\,\frac{dE_\eta(z)}{dz}+P_{\gamma\eta}\,E_\eta(z)\right]+Y_{\gamma\eta}\,\frac{dE_\eta(z)}{dz}+W_{\gamma\eta}\,E_\eta(z)=\mathbf{0}$$
$$\gamma,\eta=1,2. \quad (29)$$

Los pasos para obtener esta ecuación son similares a los descritos en [27] donde se reportó una ESLM que describe la propagación de ondas electromagnéticas en un medio anisotrópico. Como es natural, en el desarrollo para obtener la ecuación (29) se deben tener en cuenta las nuevas relaciones constitutivas: Eq. (23) y Eq. (24). Esto implica que al aplicar la ley de Ampère (ver Ref. [27]) debemos hacer uso también de la ley de Faraday $\nabla\times\overline{E}=-\frac{\partial}{\partial t}\overline{B}$ para sustituir la derivada temporal de $\overline{B}$ por las derivadas espaciales presentes en el rotor de $\overline{E}$.

A continuación aparecen expresadas las matrices $\mathbf{B}(z)$, $\mathbf{P}(z)$, $\mathbf{Y}(z)$ y $\mathbf{W}(z)$ de orden 2×2 que forman parte de (29). Es fácil comprobar que estas matrices y la ESLM derivan en las correspondientes al caso anisotrópico [27] cuando los tensores $\hat{\xi}$ y $\hat{\zeta}$ son nulos. En los cálculos se consideraron no nulos los nueve elementos de cada uno de los tensores presentes en las relaciones (21) y (22) así como también los elementos del tensor de conductividad eléctrica ($\hat{\sigma}$). Los tensores $\hat{\varepsilon}$, $\hat{\mu}$ y $\hat{\sigma}$ fueron considerados simétricos. De esta forma, las expresiones obtenidas pueden ser utilizadas directamente, sin necesidad de llevar los tensores a ejes principales previamente.

$$\mathbf{B}(z)=\begin{pmatrix}(C_2+C_{2bb})\frac{(C_2+C_{2b})}{(C_1+C_{1b})}-\hat{\nu}_{22} & \hat{\nu}_{12}+(C_2+C_{2bb})\frac{(C_3+C_{3b})}{(C_1+C_{1b})}\\ \hat{\nu}_{12}+(C_2+C_{2b})\frac{(C_3+C_{3bb})}{(C_1+C_{1b})} & (C_3+C_{3bb})\frac{(C_3+C_{3b})}{(C_1+C_{1b})}-\hat{\nu}_{11}\end{pmatrix}; \quad (30)$$

$$\mathbf{P}(z)=\begin{pmatrix}i\left[\kappa_2\hat{\nu}_{23}-\omega\hat{\tau}_{21}-(C_2+C_{2bb})\frac{(C_4+C_{4b})}{(C_1+C_{1b})}\right] & -i\left[\kappa_1\hat{\nu}_{23}+\omega\hat{\tau}_{22}+(C_2+C_{2bb})\frac{(C_5+C_{5b})}{(C_1+C_{1b})}\right]\\ -i\left[\kappa_2\hat{\nu}_{13}-\omega\hat{\tau}_{11}+(C_3+C_{3bb})\frac{(C_4+C_{4b})}{(C_1+C_{1b})}\right] & i\left[\kappa_1\hat{\nu}_{13}+\omega\hat{\tau}_{12}-(C_3+C_{3bb})\frac{(C_5+C_{5b})}{(C_1+C_{1b})}\right]\end{pmatrix}; \quad (31)$$

$$\mathbf{Y}(z)=\begin{pmatrix}i\left[\kappa_2\hat{\nu}_{23}+\omega\hat{\chi}_{12}-(C_2+C_{2b})\frac{(C_4+C_{4bb})}{(C_1+C_{1b})}\right] & -i\left[\kappa_2\hat{\nu}_{13}+\omega\hat{\chi}_{11}+(C_3+C_{3b})\frac{(C_4+C_{4bb})}{(C_1+C_{1b})}\right]\\ -i\left[\kappa_1\hat{\nu}_{23}-\omega\hat{\chi}_{22}+(C_2+C_{2b})\frac{(C_5+C_{5bb})}{(C_1+C_{1b})}\right] & i\left[\kappa_1\hat{\nu}_{13}-\omega\hat{\chi}_{21}-(C_3+C_{3b})\frac{(C_5+C_{5bb})}{(C_1+C_{1b})}\right]\end{pmatrix}; \quad (32)$$

$$\mathbf{W}(z) = \begin{pmatrix} \left[(C_7 + C_{7b}) - (C_4 + C_{4bb})\frac{(C_4+C_{4b})}{(C_1+C_{1b})}\right] & -\left[(C_6 + C_{6b}) + (C_4 + C_{4bb})\frac{(C_5+C_{5b})}{(C_1+C_{1b})}\right] \\ -\left[(C_6 + C_{6bb}) + (C_4 + C_{4b})\frac{(C_5+C_{5bb})}{(C_1+C_{1b})}\right] & \left[(C_8 + C_{8b}) - (C_5 + C_{5bb})\frac{(C_5+C_{5b})}{(C_1+C_{1b})}\right] \end{pmatrix}. \tag{33}$$

Los coeficientes C_1 a C_8 corresponden con el de un sistema anisotrópico y fueron reportados en [27]:

$$\begin{aligned}
C_1 &= \kappa_2^2\hat{\nu}_{11} - 2\kappa_1\kappa_2\hat{\nu}_{12} + \kappa_1^2\hat{\nu}_{22} - \omega^2\left(\hat{\varepsilon}_{33} + i\frac{\hat{\sigma}_{33}}{\omega}\right);\\
C_2 &= \kappa_1\hat{\nu}_{22} - \kappa_2\hat{\nu}_{12};\\
C_3 &= \kappa_2\hat{\nu}_{11} - \kappa_1\hat{\nu}_{12};\\
C_4 &= \kappa_1\kappa_2\hat{\nu}_{23} - \kappa_2^2\hat{\nu}_{13} - \omega^2\left(\hat{\varepsilon}_{13} + i\frac{\hat{\sigma}_{13}}{\omega}\right);\\
C_5 &= \kappa_1\kappa_2\hat{\nu}_{13} - \kappa_1^2\hat{\nu}_{23} - \omega^2\left(\hat{\varepsilon}_{23} + i\frac{\hat{\sigma}_{23}}{\omega}\right);\\
C_6 &= \kappa_1\kappa_2\hat{\nu}_{33} + \omega^2\left(\hat{\varepsilon}_{12} + i\frac{\hat{\sigma}_{12}}{\omega}\right);\\
C_7 &= \kappa_2^2\hat{\nu}_{33} - \omega^2\left(\hat{\varepsilon}_{11} + i\frac{\hat{\sigma}_{11}}{\omega}\right);\\
C_8 &= \kappa_1^2\hat{\nu}_{33} - \omega^2\left(\hat{\varepsilon}_{22} + i\frac{\hat{\sigma}_{22}}{\omega}\right).
\end{aligned} \tag{34}$$

Nótese que considerar la conductividad es equivalente a sustituir el tensor permitividad $\hat{\boldsymbol{\varepsilon}}$ por la permitividad compleja $\tilde{\boldsymbol{\varepsilon}}$ que es un tensor cuyos elementos son $\tilde{\varepsilon}_{nm} = \hat{\varepsilon}_{nm} + i\frac{\hat{\sigma}_{nm}}{\omega}$.

Los coeficientes C_{1b} a C_{8b} y C_{2bb} a C_{6bb} se deben a la bianisotropía:

$$C_{1b} = -\omega^2(\hat{\xi}\cdot\hat{\tau})_{33} + \omega\kappa_1(\hat{\chi}_{32} - \hat{\tau}_{23}) + \omega\kappa_2(\hat{\tau}_{13} - \hat{\chi}_{31});$$

$$\begin{aligned} C_{2b} &= \omega\hat{\chi}_{32};\\ C_{2bb} &= -\omega\hat{\tau}_{23};\end{aligned}$$

$$\begin{aligned} C_{3b} &= -\omega\hat{\chi}_{31};\\ C_{3bb} &= \omega\hat{\tau}_{13};\end{aligned}$$

$$\begin{aligned} C_{4b} &= -\omega^2(\hat{\xi}\cdot\hat{\tau})_{31} - \omega\kappa_1\hat{\tau}_{21} + \omega\kappa_2\hat{\tau}_{11} + \omega\kappa_2\hat{\chi}_{33};\\ C_{4bb} &= -\omega^2(\hat{\xi}\cdot\hat{\tau})_{13} + \omega\kappa_1\hat{\chi}_{12} - \omega\kappa_2\hat{\chi}_{11} - \omega\kappa_2\hat{\tau}_{33}; \end{aligned} \tag{35}$$

$$\begin{aligned} C_{5b} &= -\omega^2(\hat{\xi}\cdot\hat{\tau})_{32} - \omega\kappa_1\hat{\tau}_{22} + \omega\kappa_2\hat{\tau}_{12} - \omega\kappa_1\hat{\chi}_{33};\\ C_{5bb} &= -\omega^2(\hat{\xi}\cdot\hat{\tau})_{23} + \omega\kappa_1\hat{\chi}_{22} - \omega\kappa_2\hat{\chi}_{21} + \omega\kappa_1\hat{\tau}_{33};\end{aligned}$$

$$\begin{aligned} C_{6b} &= \omega^2(\hat{\xi}\cdot\hat{\tau})_{12} + \omega\kappa_2\hat{\tau}_{32} + \omega\kappa_1\hat{\chi}_{13};\\ C_{6bb} &= \omega^2(\hat{\xi}\cdot\hat{\tau})_{21} - \omega\kappa_2\hat{\chi}_{23} - \omega\kappa_1\hat{\tau}_{31}; \end{aligned} \tag{36}$$

$$C_{7b} = -\omega^2(\hat{\xi}\cdot\hat{\tau})_{11} + \omega\kappa_2(\hat{\chi}_{13} - \hat{\tau}_{31});$$

$$C_{8b} = -\omega^2(\hat{\xi}\cdot\hat{\tau})_{22} + \omega\kappa_1(\hat{\tau}_{32} - \hat{\chi}_{23}). \tag{37}$$

A partir de las expresiones anteriores se pueden determinar condiciones de simetría para los tensores presentes en las relaciones (21) y (22) que de cumplirse darían lugar a un operador Sturm-Liouville formalmente hermítico es decir, se cumpliría que $\mathbf{B} = \mathbf{B}^\dagger, \mathbf{W} = \mathbf{W}^\dagger, \mathbf{Y} = -\mathbf{P}^\dagger$. Las siguientes condiciones son suficientes:

- $\hat{\varepsilon}$ y $\hat{\mu}$ reales y simétricos, $\hat{\xi} = \hat{\zeta}^\dagger$ y $\hat{\sigma} = \mathbf{0}$.

El símbolo † sobre la matrix significa su traspuesta conjugada. Si se cumplen las condiciones de hermiticidad formal, entonces los eigenvalores del operador Sturm-Liouville podrán ser reales o aparecerán en pares del tipo: k_ℓ y su complejo conjugado.

El cálculo de las correspondientes componentes de la forma diferencial lineal $A_\gamma = B_{\gamma\eta}\,\frac{dE_\eta(z)}{dz} + P_{\gamma\eta}\,E_\eta(z)$ presentes en la ecuación (29) conduce a $A_1(z) = -i\omega H_2(z)$ y $A_2(z) = i\omega H_1(z)$. Este resultado asocia directamente la propiedad de continuidad de $\mathbf{A}(z)$ con la continuidad de las componentes transversales H_1, H_2 del campo magnético. El mismo resultado fue reportado en [27] para el caso del medio anisotrópico.

La búsqueda de soluciones linealmente independientes (LI) del sistema diferencial (29) en un dominio homogéneo conduce al planteamiento de un problema cuadrático de eigenvalores [28]. Un análisis detallado de la solución de este problema para la ESLM se puede encontrar en [10]. A continuación solo se presentan algunos elementos básicos que serán de utilidad para expresar una función de Green para los medios bianisotrópicos que abordamos a modo de ejemplo en la secciones siguientes.

Para un dominio homogéneo, las soluciones LI del sistema diferencial (29) pueden expresarse en forma de exponenciales:

$$\overline{E}_\perp = \overline{E}_{0\perp} e^{ikz}, \tag{38}$$

siendo $\overline{E}_\perp = [E_1, E_2]^T$ el vector que involucra las componentes transversales del campo eléctrico, en correspondencia con la Eq. (29). Los eigenvalores k se obtienen a partir de los ceros del determinante de la matriz secular:

$$\mathbf{Q}(k) = -k^2\mathbf{B} + ik(\mathbf{P} + \mathbf{Y}) + \mathbf{W}. \tag{39}$$

Si la matrix $\mathbf{B}$ es regular tendremos un conjunto $K = \{k_j, j = 1,2,3,4\}$ de cuatro eigenvalores ($\mathbf{Q}(k)$ resulta un polinomio de cuarto orden en k).

En [10] se reportó una forma general y compacta para la función de Green ($\mathbf{G}(z,z')$) regular en el infinito para el operador Sturm-Liouville matricial homogéneo. La homogeneidad significa que los parámetros que involucrados en los coeficientes matriciales ($\mathbf{B}$, $\mathbf{P}$, $\mathbf{Y}$ y $\mathbf{W}$) no dependen de la posición. Esta forma general de $\mathbf{G}(z,z')$ admite dos simplificaciones importantes cuando los eigenvalores k_j aparecen por pares del tipo $(k_j, -k_j)$, una para los problemas con $\mathbf{P} + \mathbf{Y} = \mathbf{0}$ y la otra para los problemas con $\mathbf{P} + \mathbf{Y} \neq \mathbf{0}$. En las secciones siguientes presentaremos ambas simplificaciones.

3.2 Medios magnetoeléctricos

Según Kong [24] los materiales magnetoeléctricos fueron predichos teóricamente por Dzyaloshinskii [12] y Landau y Lifshitz [14] y observados experimentalmente en 1960 por Astrov [11] en óxido de cromo antiferromagnético. Para estos medios Dzyaloshinskii propuso las siguientes relaciones constitutivas:

$$\overline{D} = \begin{pmatrix} \varepsilon & 0 & 0 \\ 0 & \varepsilon & 0 \\ 0 & 0 & \varepsilon_z \end{pmatrix} \cdot \overline{E} + \begin{pmatrix} \xi & 0 & 0 \\ 0 & \xi & 0 \\ 0 & 0 & \xi_z \end{pmatrix} \cdot \overline{H} \tag{40}$$

$$\overline{B} = \begin{pmatrix} \xi & 0 & 0 \\ 0 & \xi & 0 \\ 0 & 0 & \xi_z \end{pmatrix} \cdot \overline{E} + \begin{pmatrix} \mu & 0 & 0 \\ 0 & \mu & 0 \\ 0 & 0 & \mu_z \end{pmatrix} \cdot \overline{H} \,. \tag{41}$$

En este caso las matrices **B**, **P** y **Y** resultan:

$$\mathbf{B} = \begin{pmatrix} -\frac{1}{\mu} + \frac{{\kappa_1}^2}{\mu^2\left(\frac{{\kappa_1}^2}{\mu} + \frac{{\kappa_2}^2}{\mu} + \frac{{\xi_z}^2\omega^2}{\mu_z} - \left(\varepsilon_z + \frac{i\sigma_z}{\omega}\right)\omega^2\right)} & \frac{\kappa_1\kappa_2}{\mu^2\left(\frac{{\kappa_1}^2}{\mu} + \frac{{\kappa_2}^2}{\mu} + \frac{{\xi_z}^2\omega^2}{\mu_z} - \left(\varepsilon_z + \frac{i\sigma_z}{\omega}\right)\omega^2\right)} \\ \frac{\kappa_1\kappa_2}{\mu^2\left(\frac{{\kappa_1}^2}{\mu} + \frac{{\kappa_2}^2}{\mu} + \frac{{\xi_z}^2\omega^2}{\mu_z} - \left(\varepsilon_z + \frac{i\sigma_z}{\omega}\right)\omega^2\right)} & -\frac{1}{\mu} + \frac{{\kappa_2}^2}{\mu^2\left(\frac{{\kappa_1}^2}{\mu} + \frac{{\kappa_2}^2}{\mu} + \frac{{\xi_z}^2\omega^2}{\mu_z} - \left(\varepsilon_z + \frac{i\sigma_z}{\omega}\right)\omega^2\right)} \end{pmatrix}; \tag{42}$$

$$\mathbf{P} = \begin{pmatrix} -\frac{i\kappa_1\left(-\frac{\kappa_2\xi\omega}{\mu} + \frac{\kappa_2\xi_z\omega}{\mu_z}\right)}{\mu\left(\frac{{\kappa_1}^2}{\mu} + \frac{{\kappa_2}^2}{\mu} + \frac{{\xi_z}^2\omega^2}{\mu_z} - \left(\varepsilon_z + \frac{i\sigma_z}{\omega}\right)\omega^2\right)} & -i\left(-\frac{\xi\omega}{\mu} + \frac{\kappa_1\left(\frac{\kappa_1\xi\omega}{\mu} - \frac{\kappa_1\xi_z\omega}{\mu_z}\right)}{\mu\left(\frac{{\kappa_1}^2}{\mu} + \frac{{\kappa_2}^2}{\mu} + \frac{{\xi_z}^2\omega^2}{\mu_z} - \left(\varepsilon_z + \frac{i\sigma_z}{\omega}\right)\omega^2\right)}\right) \\ -i\left(\frac{\xi\omega}{\mu} + \frac{\kappa_2\left(-\frac{\kappa_2\xi\omega}{\mu} + \frac{\kappa_2\xi_z\omega}{\mu_z}\right)}{\mu\left(\frac{{\kappa_1}^2}{\mu} + \frac{{\kappa_2}^2}{\mu} + \frac{{\xi_z}^2\omega^2}{\mu_z} - \left(\varepsilon_z + \frac{i\sigma_z}{\omega}\right)\omega^2\right)}\right) & -\frac{i\kappa_2\left(\frac{\kappa_1\xi\omega}{\mu} - \frac{\kappa_1\xi_z\omega}{\mu_z}\right)}{\mu\left(\frac{{\kappa_1}^2}{\mu} + \frac{{\kappa_2}^2}{\mu} + \frac{{\xi_z}^2\omega^2}{\mu_z} - \left(\varepsilon_z + \frac{i\sigma_z}{\omega}\right)\omega^2\right)} \end{pmatrix}; \tag{43}$$

$$\mathbf{Y} = \begin{pmatrix} -\frac{i\kappa_1\left(-\frac{\kappa_2\xi\omega}{\mu}+\frac{\kappa_2\xi_z\omega}{\mu_z}\right)}{\mu\left(\frac{\kappa_1{}^2}{\mu}+\frac{\kappa_2{}^2}{\mu}+\frac{\xi_z{}^2\omega^2}{\mu_z}-\left(\varepsilon_z+\frac{i\sigma_z}{\omega}\right)\omega^2\right)} & -i\left(\frac{\xi\omega}{\mu}+\frac{\kappa_2\left(-\frac{\kappa_2\xi\omega}{\mu}+\frac{\kappa_2\xi_z\omega}{\mu_z}\right)}{\mu\left(\frac{\kappa_1{}^2}{\mu}+\frac{\kappa_2{}^2}{\mu}+\frac{\xi_z{}^2\omega^2}{\mu_z}-\left(\varepsilon_z+\frac{i\sigma_z}{\omega}\right)\omega^2\right)}\right) \\ -i\left(-\frac{\xi\omega}{\mu}+\frac{\kappa_1\left(\frac{\kappa_1\xi\omega}{\mu}-\frac{\kappa_1\xi_z\omega}{\mu_z}\right)}{\mu\left(\frac{\kappa_1{}^2}{\mu}+\frac{\kappa_2{}^2}{\mu}+\frac{\xi_z{}^2\omega^2}{\mu_z}-\left(\varepsilon_z+\frac{i\sigma_z}{\omega}\right)\omega^2\right)}\right) & -\frac{i\kappa_2\left(\frac{\kappa_1\xi\omega}{\mu}-\frac{\kappa_1\xi_z\omega}{\mu_z}\right)}{\mu\left(\frac{\kappa_1{}^2}{\mu}+\frac{\kappa_2{}^2}{\mu}+\frac{\xi_z{}^2\omega^2}{\mu_z}-\left(\varepsilon_z+\frac{i\sigma_z}{\omega}\right)\omega^2\right)} \end{pmatrix}; \tag{44}$$

En tanto que los elementos de $\mathbf{W}$ son:

$$\begin{aligned}
W_{11} &= \frac{\kappa_2{}^2}{\mu_z}+\frac{\xi^2\omega^2}{\mu}-\left(\varepsilon+\frac{i\sigma}{\omega}\right)\omega^2-\frac{\left(-\frac{\kappa_2\xi\omega}{\mu}+\frac{\kappa_2\xi_z\omega}{\mu_z}\right)^2}{\frac{\kappa_1{}^2}{\mu}+\frac{\kappa_2{}^2}{\mu}+\frac{\xi_z{}^2\omega^2}{\mu_z}-\left(\varepsilon_z+\frac{i\sigma_z}{\omega}\right)\omega^2}; \\
W_{12} &= -\frac{\kappa_1\kappa_2}{\mu_z}-\frac{\left(\frac{\kappa_1\xi\omega}{\mu}-\frac{\kappa_1\xi_z\omega}{\mu_z}\right)\left(-\frac{\kappa_2\xi\omega}{\mu}+\frac{\kappa_2\xi_z\omega}{\mu_z}\right)}{\frac{\kappa_1{}^2}{\mu}+\frac{\kappa_2{}^2}{\mu}+\frac{\xi_z{}^2\omega^2}{\mu_z}-\left(\varepsilon_z+\frac{i\sigma_z}{\omega}\right)\omega^2}; \\
W_{21} &= -\frac{\kappa_1\kappa_2}{\mu_z}-\frac{\left(\frac{\kappa_1\xi\omega}{\mu}-\frac{\kappa_1\xi_z\omega}{\mu_z}\right)\left(-\frac{\kappa_2\xi\omega}{\mu}+\frac{\kappa_2\xi_z\omega}{\mu_z}\right)}{\frac{\kappa_1{}^2}{\mu}+\frac{\kappa_2{}^2}{\mu}+\frac{\xi_z{}^2\omega^2}{\mu_z}-\left(\varepsilon_z+\frac{i\sigma_z}{\omega}\right)\omega^2}; \\
W_{22} &= \frac{\kappa_1{}^2}{\mu_z}+\frac{\xi^2\omega^2}{\mu}-\left(\varepsilon+\frac{i\sigma}{\omega}\right)\omega^2-\frac{\left(\frac{\kappa_1\xi\omega}{\mu}-\frac{\kappa_1\xi_z\omega}{\mu_z}\right)^2}{\frac{\kappa_1{}^2}{\mu}+\frac{\kappa_2{}^2}{\mu}+\frac{\xi_z{}^2\omega^2}{\mu_z}-\left(\varepsilon_z+\frac{i\sigma_z}{\omega}\right)\omega^2}.
\end{aligned} \tag{45}$$

A modo ilustrativo se consideró:

$$\hat{\sigma} = \begin{pmatrix} \sigma & 0 & 0 \\ 0 & \sigma & 0 \\ 0 & 0 & \sigma_z \end{pmatrix}. \tag{46}$$

Como es de esperar, para $\hat{\sigma} = \mathbf{0}$ se cumplen las condiciones de hermiticidad formal del operador Sturm-Liouville matricial:

$$\begin{aligned}
\mathbf{B} &= \mathbf{B}^\dagger; \\
\mathbf{W} &= \mathbf{W}^\dagger; \\
\mathbf{Y} &= -\mathbf{P}^\dagger.
\end{aligned} \tag{47}$$

Se puede verificar que en este caso el determinante de la matriz secular $\mathbf{Q}(k)$ solo contiene potencias pares de k, lo que significa que los eigenvalores también formarán pares del tipo $(k_j, -k_j)$. Para este ejemplo tenemos que $\mathbf{P}+\mathbf{Y} \neq \mathbf{0}$ de modo que la función de Green $\mathbf{G}(z,z')$ admite la siguiente simplificación [10]:

$$\mathbf{G}(z,z') = \sum_{k_j \in K_\uparrow;\ j=1,2} i \frac{\mathbf{C}_o^T(\mathrm{sgn}(z-z')\cdot k_j)}{D'(k_j)}\, e^{ik_j|z-z'|}\,, \qquad (48)$$

donde $\mathbf{C}_o(k)$ es la matriz de cofactores de la matriz secular $\mathbf{Q}(k)$ y $\mathbf{C}_o^T(k)$ es su traspuesta. Nótese que esta matrix es evaluada en k_j multiplicado por la función signo $\mathbf{sgn}$ de argumento $z-z'$. El denominador $D'(k)$ es el polinomio en k que resulta de derivar el polinimio secular $\mathbf{Det}[\mathbf{Q}(k)]$ con respecto a k. Los eigenvalores k_j generalmente son complejos, y el subconjunto $K_\uparrow$ incluye los eigenvalores con parte imaginaria positiva. Si alguna de las parejas $(k_j, -k_j)$ fuera real, se toma el eigenvalor positivo para evaluar (48).

3.3 Resonador de anillo partido

Un "Resonador de anillo partido" (Split-Ring Resonator, SRR) es una estructura producida artificialmente que consiste en dos anillos metálicos concéntricos abiertos en extremos opuestos y su diseño fue sugerido por Pendry et al. en 1999 [29] como un material que exhibe una permeabilidad magnética $\mu < 0$ alrededor de la frecuencia de resonancia magnética. Los metamateriales cuyos bloques básicos presentan estas estructuras pueden exhibir respuestas electromagnéticas efectivas exóticas que incluyen pero no se limitan a índices de refraccción negativos o cercanos a cero [30, 31, 32]. El SRR puede ser modelado como un medio bianisotrópico con las siguientes relaciones constitutivas [24, 33, 34]:

$$\overline{D} = \begin{pmatrix} \varepsilon_x & 0 & 0 \\ 0 & \varepsilon_y & 0 \\ 0 & 0 & \varepsilon_z \end{pmatrix} \cdot \overline{E} + \begin{pmatrix} 0 & 0 & 0 \\ 0 & 0 & 0 \\ 0 & -i\xi_0 & 0 \end{pmatrix} \cdot \overline{H}; \qquad (49)$$

$$\overline{B} = \begin{pmatrix} 0\,0 & 0 \\ 0\,0 & +i\xi_0 \\ 0\,0 & 0 \end{pmatrix} \cdot \overline{E} + \begin{pmatrix} \mu_x & 0 & 0 \\ 0 & \mu_y & 0 \\ 0 & 0 & \mu_z \end{pmatrix} \cdot \overline{H}. \tag{50}$$

En este caso las matrices **B**, **P**, **Y** y **W** resultan:

$$\mathbf{B} = \begin{pmatrix} -\frac{1}{\mu_y} + \frac{\left(\frac{\kappa_1}{\mu_y} - \frac{i\xi_0\omega}{\mu_y}\right)\left(\frac{\kappa_1}{\mu_y} + \frac{i\xi_0\omega}{\mu_y}\right)}{\frac{\kappa_2{}^2}{\mu_x} + \frac{\kappa_1{}^2}{\mu_y} - \varepsilon_z\omega^2 + \frac{\xi_0{}^2\omega^2}{\mu_y}} & \frac{\kappa_2\left(\frac{\kappa_1}{\mu_y} + \frac{i\xi_0\omega}{\mu_y}\right)}{\mu_x\left(\frac{\kappa_2{}^2}{\mu_x} + \frac{\kappa_1{}^2}{\mu_y} - \varepsilon_z\omega^2 + \frac{\xi_0{}^2\omega^2}{\mu_y}\right)} \\ \\ \frac{\kappa_2\left(\frac{\kappa_1}{\mu_y} - \frac{i\xi_0\omega}{\mu_y}\right)}{\mu_x\left(\frac{\kappa_2{}^2}{\mu_x} + \frac{\kappa_1{}^2}{\mu_y} - \varepsilon_z\omega^2 + \frac{\xi_0{}^2\omega^2}{\mu_y}\right)} & -\frac{1}{\mu_x} + \frac{\kappa_2{}^2}{\mu_x{}^2\left(\frac{\kappa_2{}^2}{\mu_x} + \frac{\kappa_1{}^2}{\mu_y} - \varepsilon_z\omega^2 + \frac{\xi_0{}^2\omega^2}{\mu_y}\right)} \end{pmatrix}; \tag{51}$$

$$\mathbf{P} = \mathbf{0}; \tag{52}$$

$$\mathbf{Y} = \mathbf{0}; \tag{53}$$

$$\mathbf{W} = \begin{pmatrix} \frac{\kappa_2{}^2}{\mu_z} - \varepsilon_x\omega^2 & -\frac{\kappa_1\kappa_2}{\mu_z} \\ \\ -\frac{\kappa_1\kappa_2}{\mu_z} & \frac{\kappa_1{}^2}{\mu_z} - \varepsilon_y\omega^2 \end{pmatrix}. \tag{54}$$

Se puede verificar de forma simple y directa que en este caso donde hemos considerado $\hat{\sigma} = \mathbf{0}$, también se cumplen las condiciones de hermiticidad formal del operador Sturm-Liouville matricial. Dado que $\mathbf{P} + \mathbf{Y} = \mathbf{0}$ queda claro que el determinante secular solo tendrá potencias pares de k, lo que significa que los eigenvalores también formarán pares del tipo $(k_j, -k_j)$. Para este problema donde $\mathbf{P} + \mathbf{Y} = \mathbf{0}$ la función de Green $\mathbf{G}(z, z')$ admite la siguiente simplificación [10]:

$$\mathbf{G}(z, z') = \sum_{k_j \in K_\uparrow;\ j=1,2} i\frac{\mathbf{C}_o^T(k_j)}{D'(k_j)} e^{ik_j|z-z'|}. \tag{55}$$

En este ejemplo las expresiones analíticas son más sencillas que en el ejemplo anterior, y se tiene que:

$$\mathbf{G}(z,z') = \frac{i}{k_1\left(4\mathrm{Det}[\mathbf{B}]k_1^2 - 2M\right)} \begin{pmatrix} -B_{22}k_1^2 + W_{22} & B_{12}k_1^2 - W_{12} \\ B_{21}k_1^2 - W_{21} & -B_{11}k_1^2 + W_{11} \end{pmatrix} e^{ik_1|z-z'|} + \frac{i}{k_2\left(4\mathrm{Det}[\mathbf{B}]k_2^2 - 2M\right)} \begin{pmatrix} -B_{22}k_2^2 + W_{22} & B_{12}k_2^2 - W_{12} \\ B_{21}k_2^2 - W_{21} & -B_{11}k_2^2 + W_{11} \end{pmatrix} e^{ik_2|z-z'|}, \tag{56}$$

con:

$$k_1 = +\sqrt{\frac{M + \sqrt{M^2 - 4\mathrm{Det}[\mathbf{B}]\mathrm{Det}[\mathbf{W}]}}{2\mathrm{Det}[\mathbf{B}]}};$$
$$k_2 = +\sqrt{\frac{M - \sqrt{M^2 - 4\mathrm{Det}[\mathbf{B}]\mathrm{Det}[\mathbf{W}]}}{2\mathrm{Det}[\mathbf{B}]}}, \tag{57}$$

donde $M = B_{22}W_{11} + B_{11}W_{22} - B_{21}W_{12} - B_{12}W_{21}$, involucra los cuatro elementos matriciales de $\mathbf{B}$ y $\mathbf{W}$. Con $\mathrm{Det}[\mathbf{B}]$ denotamos el determinante de la matrix $\mathbf{B}$ y de igual forma para $\mathbf{W}$.

4 Conclusiones

Como dijimos en la Introducción, hemos analizado dos excitaciones elementales de la mayor importancia en sistemas a capas plano paralelas para concluir que se describen mediante sendos problemas de Sturm-Liouville matriciales. Estas son las oscilaciones elásticas y los modos electromagnéticos cuando los materiales que componen la estructura tienen bianisotropía.

Para cada uno de ellos hemos reportado explícitamente las matrices $\mathbf{B},\mathbf{P},\mathbf{Y},\mathbf{W}$ que entran en el problema de Sturm-Liouville y hemos analizado bajo qué condiciones estas matrices hacen que el operador sea formalmente hermítico. En los casos estudiados solo la presencia de mecanismos de pérdida como la conductividad hacen que el operador no tenga esta importante propiedad.

Las funciones de Green regulares en el infinito de estos problemas solo pueden tener dos formas o estructuras. [10] Estas vienen determinadas simplemente por el hecho de que la matriz $\mathbf{P}+\mathbf{Y}$ sea o no sea nula. Para los dos casos estudiados hemos podido

aportar este importante dato de sus funciones de Green regulares en el infinito.

Agradecimientos

R. Pérez-Álvarez agradece la hospitalidad de los colegas de la Universidad de La Habana (Cuba) y a F. García-Moliner de la Universidad Jaume I, Castellón, España, donde se esbozaron las primeras ideas del presente trabajo. R. Pernas-Salomón agradece el apoyo de la beca PRODEP No. DSA/103.5/16/9408 y la hospitalidad de los colegas del Instituto de Física "Luis Rivera Terrazas" de la Benemérita Universidad Autónoma de Puebla (BUAP).

Bibliografía

1. G. Bastard, "Wave mechanics applied to semiconductor heterostructures", Éditions de Physique, Paris (1989).
2. B. Vinter and C. Weisbuch, "Quantum Semiconductor Structures", Academic Press, San Diego (1991).
3. F García-Moliner and VR Velasco, "Theory of Single and Multiple Interfaces", World Scientific, Singapore (1992).
4. F. García-Moliner, R. Pérez-Alvarez, J. Fernández-Velicia and L. Chico Gómez, "Electrones y Fonones en Pozos Cuánticos", edited by Universidad Nacional de Educación a Distancia (UNED), Madrid, Spain (1994).
5. C Trallero-Giner, R Pérez-Álvarez and F García-Moliner, "Long wave polar modes in semiconductor heterostructures", Elsevier Science (1998).
6. R Pérez-Álvarez and F García-Moliner, "Transfer matrix, Green Function and related techniques: Tools for the study of multilayer heterostructures", Universitat Jaume I, Castellón de la Plana, Spain (2004).
7. R Pernas Salomón, "Problema de sturm-liouville matricial en el estudio de diversas excitaciones elementales en sistemas a capas", Tesis de Doctorado, Universidad Autónoma del Estado de Morelos, México, junio de 2015.
8. R. Pérez-Álvarez and R. Pernas-Salomón, "Ubiquity of the Sturm-Liouville problem in multilayer systems", EPL (Europhysics Letters) 115:1, pp 10 (2016).
9. B Friedman, "Principles and techniques of applied mathematics", J Wiley, New York (1956).
10. René Pernas-Salomón and R. Pérez-Álvarez and V.R. Velasco, "General form of the Green s function regular at infinity for the homogeneous Sturm Liouville matrix operator", Appl. Math. and Comput. 269, 824 - 833, (2015).
11. D.N. Astrov, "The magnetoelectric effect in antiferromagnetics", Zh. Eksp. Teor. Fiz., vol. 38, 984-985 (1960).
12. I.E. Dzyaloshinskii, "On the magnetoelectrical effect in antiferromagnets, Soviet Physics JETP, vol. 10, 628-629 (1960).
13. V.L. Inderbom, "Irreducible representations of the magnetic groups and allowance for magnetic symmetry", Soviet Phys. Crystallogr., vol. 5, 493 (1960).

14. L.D. Landau and E.M. Lifschitz, " Electrodynamics of Continuous Media", Addison Wesley, Massachusetts, USA, (1960).
15. R.R. Birss, "Macroscopic symmetry in space-time", Rep. Prog. Phys., vol. 26, 307-310 (1963).
16. R.R. Birss and R.G. Shrubsall, "The propagation of EM waves in magnetoelectric crystals", Phil. Mag., vol. 15, 687-700 (1967).
17. G.T. Rado, "Observation and possible mechanisms of magnetoelectric effects in a ferromagnet", Phys. Rev. Lett., vol. 13, 355 (1967).
18. Kaiser S. Kunz, "Plane electromagnetic waves in moving media and reflections from moving interfaces", Journal of Applied Physics, vol. 51, no. 2, 873-884 (1980).
19. D. Censor, "Dispersion equations in moving media", Proceedings of the IEEE, vol. 68, no. 4, 528-529 (1980).
20. Friedrich W. Hehl and Yuri N. Obukhov and Jean-Pierre Rivera and Hans Schmid, "Relativistic analysis of magnetoelectric crystals: Extracting a new 4-dimensional P odd and T odd pseudoscalar from Cr2O3 data", Physics Letters A, vol. 372, no. 8, 1141-1146 (2008).
21. Yuri N. Obukhov and Friedrich W. Hehl, "Forces and momenta caused by electromagnetic waves in magnetoelectric media", Physics Letters A, vol. 372, no. 22, 3946 - 3952 (2008).
22. Young-Sea Huang, "A new perspective on relativistic transformation versus the conventional Lorentz transformation illustrated by the problem of electromagnetic waves in moving media", Physica Scripta, vol. 81, no. 1, 015004 (2010).
23. J.A. Kong, "Electromagnetic waves in moving media", PhD thesis, Syracuse University (1968).
24. J.A. Kong, "Electromagnetic Wave Theory", Cambridge, Massachusetts, USA, EMW Publishing, isbn = 0-9668143-9-8 (2008).
25. Lei Chen, Zhenya Lei, Rui Yang, Xiaowei Shi, and Jiawei Zhang, "Determining the effective electromagnetic parameters of bianisotropic metamaterials with periodic structures", Progress in Electromagneic Research M, Vol. 29, 79-93 (2013).
26. Po-Han Chang, Chih-Yu Kuo, and Ruey-Lin Chern, "Wave propagation in bianisotropic metamaterials: angular selective transmission", Optics Express, Vol. 22, No. 21, 25710-25721 (2014).
27. R. Pernas-Salomón and R. Pérez-Álvarez, "Sturm-liouville matrix equation for the study of electromagnetic waves propagation in layered anisotropic media", Progress In Electromagnetics Research M (PIER M) 40, 79-90 (2014).
28. Tisseur, F. and Meerbergen, K., "The Quadratic Eigenvalue Problem",SIAM Review 43:2, 235-286, (2001).
29. J. B. Pendry, A. J. Holden, D. J. Robbins, and W. J. Stewart, "Magnetism from Conductors and Enhanced Nonlinear Phenomena", IEEE TRANSACTIONS ON MICROWAVE THEORY AND TECHNIQUES 47:11, 2075-2084, (1999).
30. D. R. Smith, Willie J. Padilla, D. C. Vier, S. C. Nemat-Nasser, and S. Schultz, "Composite Medium with Simultaneously Negative Permeability and Permittivity", Phys. Rev. Lett. 84:18, 4184-4187, (2000).
31. Linden, Stefan and Enkrich, Christian and Wegener, Martin and Zhou, Jiangfeng and Koschny, Thomas and Soukoulis, Costas M, "Magnetic Response of Metamaterials at 100 Terahertz", Science 306:5700, 1351-1353, (2004).
32. N. Katsarakis, G. Konstantinidis, A. Kostopoulos, R. S. Penciu, T. F. Gundogdu, M. Kafesaki, and E. N. Economou, "Magnetic response of split-ring resonators in the far-infrared frequency regime", OPTICS LETTERS 30:11, 1348-1350, (2005).
33. Xudong Chen, Bae-Ian Wu, Jin Au Kong, and Tomasz M. Grzegorczyk, "Retrieval of the effective constitutive parameters of bianisotropic metamaterials", Phys. Rev. E. 71, 046610, (2005).
34. Ugur Cem Hasar, Musa Bute, Joaquim J. Barroso, Cumali Sabah, Yunus Kaya, and Mehmet Ertugrul, "Power analysis of multilayer structures composed of conventional

materials and bi-anisotropic metamaterial slabs", J. Opt. Soc. Am. B 31:5, 939-947, (2014).

Index